

WHITE PAPER

Coupling Relations in RFID Systems II: Practical Performance Measurements

Peter Cole, Damith Ranasinghe, Behnam Jamali

AUTO-ID CENTRE UNIVERSITY OF ADELAIDE, ENGINEERING BUILDING N-204, NORTH TERRACE, ADELAIDE, SA 5005, AUSTRALIA

ABSTRACT

Reader tag coupling relations in RFID systems are an important aspect of the system development process that are often inadequately understood; nevertheless electromagnetic coupling becomes significant in the context of optimising RFID systems. Coupling volume theory provides an uncomplicated and a simple means of optimising electromagnetic coupling. This paper describes a practical application of the coupling volume theory to an antenna performance comparison, and presents the companion concept of radiation quality factor for comparing antenna performance. RFID systems are in a process of evolution and an important outcome of this process is the development of a class hierarchy where higher class labels are often battery power supported. This category of labels requires a means of turning “on” and “off” that battery support, to conserve power and thus prolong battery life. Two solutions available for the development of a turn on circuit use resonance in a label rectification circuit to provide a high sensitivity result. This paper presents the results of experiments conducted to evaluate the performance of the above class of turn on circuits.

WHITE PAPER

Coupling Relations in RFID Systems II: Practical Performance Measurements

Biographies



Professor Peter Cole
Research Director

Dr. Cole, Professor of Radio Frequency Identification (RFID) systems in the Department of Electrical and Electronic Engineering at the University of Adelaide, has been selected to head a new RFID study in Australia. Dr. Cole's current research covers the industrial applications of electromagnetic identification and tracking systems, the design of multi-function microcircuits, the design of signaling methodologies for simultaneous high-speed reading of multiple electronic labels, and the development of international standards for RFID systems. Dr. Cole will be working closely with both the MIT and Cambridge Labs. He will be focusing his research and expertise on the EPC™ concept within the silicon chips currently being prototyped by Center sponsors.



Damith Ranasinghe
Doctoral Candidate & Research Assistant

Graduated with a degree in Information Technology and Telecommunications Engineering at The University of Adelaide. Currently, Damith is a PhD candidate working at The Auto-ID Centre research group at The University of Adelaide. Current research interest include electromagnetic coupling, encryption, and authentication in RFID.



Behnam Jamali
Doctoral Candidate & Research Assistant

Graduated with a degree in Electronics Engineering at The University of Adelaide, Australia. Currently, Behnam is a PhD candidate carrying out research at The University of Adelaide's Auto-ID Centre. Research interests include low power analogue CMOS circuits, as well as design of efficient rectifiers.

WHITE PAPER

Coupling Relations in RFID Systems II: Practical Performance Measurements

Contents

1. Introduction.....	3
2. Notation	3
3. Near Field Creation Structures.....	4
3.1. Monopole Wedge Above Ground Antenna	4
3.2. Bow Tie Antennas	8
3.3. Loop Antennas.....	9
4. Coupling Volume Theory.....	18
4.1. Loop Antenna Structure.....	18
4.2. Bow Tie Antenna Structure.....	20
4.3. Antenna Comparison	20
5. Turn on Circuits	22
5.1. Concepts	22
5.2. Realistic Performance Predictions	22
6. Conclusion.....	32
7. Acknowledgement.....	32
8. References	33

1. INTRODUCTION

This paper is the second in a series dealing with coupling issues in RFID produced by staff of the Adelaide Research Laboratory of the Auto-ID Center, and can be regarded as a companion paper to that in Reference [1].

In that paper, a wide range of topics was covered, and some ideas were introduced without support from experimental results.

Two of the objectives of this paper are to provide experimental results in support of some of the concepts introduced earlier, and to proceed a little further in the extraction of some of the practical consequences of some of the theory presented.

Because electromagnetic engineering is not particularly well understood in parts of the RFID community, the experimental procedures as well as the results of the experimental work are described. This will serve to some extent an educational purpose, but will also enable better evaluation of the work presented here by experienced electromagnetic engineers.

Finally, an objective has been to re-present some of the results of the previous paper in a notation that removes possible ambiguity in the previously employed notation when the results of a wedge above ground plane antenna are related to those for a bow tie antenna.

After a brief statement of notation in Section 2, Section 3 of the paper proceeds to a further consideration of near field creation structures of both the electric field and magnetic field type. This work is of significance not only in the near field but, through the Lorenz reciprocity theorem, also in the far field when structures that are both physically and electrically small, but in other ways similar those to described here, are used as label antennas. Past experimental work in electric field creation and detection structures is clarified, and experiments to confirm the achievement of uniform currents in large loops are presented.

Section 4 returns to coupling volume theory described in detail in Reference [1], and extends that work so that two key performance parameters, namely antenna coupling volume and radiation quality factor, for both electric field and magnetic field antennas, can be explored in terms of a dimensionless parameter involving antenna size.

Section 5 considers some problems which arise in battery-operated backscatter (or indeed other forms of reply signal generation) tags, and presents experimental results for the circuits and calculates turn-on range for both low-power and zero-power varieties of turn-on circuit.

Section 6 provides a brief summary of the principal conclusions of the paper.

2. NOTATION

The notation and nomenclature used in the paper for physical quantities will be as defined in ISO 1000, [4] and a more complete description of the typography can be obtained from [1]. There are some traditional exceptions to these rules where Greek and Roman upper case symbols do not differ sufficiently.

Where possible, the results obtained from analysis will be reduced to dimensionless ratios, and the concepts employed will be those which have a physical meaning.

3. NEAR FIELD CREATION STRUCTURES

A number of field creation structures and label antenna forms were introduced in [1]. That paper contained a brief analysis of a bow tie antenna. However an ambiguity in the notation used when results of the monopole wedge above ground case are related to the bow tie antenna case may prevent a reader from interpreting the results correctly. For this reason bow tie antenna and monopole wedge above ground antenna results are summarised again with the aim of achieving greater clarity.

It has also been shown in [1] that, when an interrogator antenna takes the form of a small loop, and the objective is to maximise the magnetic field at a label position in the near field of that loop, subject to a given electromagnetic compatibility regulation enforced in the far field, and no other considerations such as antenna bandwidth or driving power are taken into account, the optimum size for a loop is that where the radius of the loop tends to zero.

However, practical consequences and constraints, such as the need to constrain the driving power to practical values, indicates that such an optimisation is misconceived, and loops of finite size must be considered.

Since such loops are known to produce near fields that diminish substantially when the interrogation distance significantly exceeds the loop radius, we are led to consider large loop antennas as label exciting systems. Such loops may suffer from non-uniformity of the current distribution, with the attendant problems of increased radiation and difficulties of tuning. In the previous paper, the suggestion of modification of loop structure to deal with these problems was made, but no analysis or experimental results were presented. It is intended in this paper to present such analysis and results.

3.1. Monopole Wedge Above Ground Antenna

Figure 1 shows a monopole wedge above ground antenna. A detailed experimental study of these antennas was first published by Brown and Woodward [8].

A three-parameter circuit model which we have obtained by analysing their results for a monopole wedge above ground is shown in Figure 2.

Figure 1a

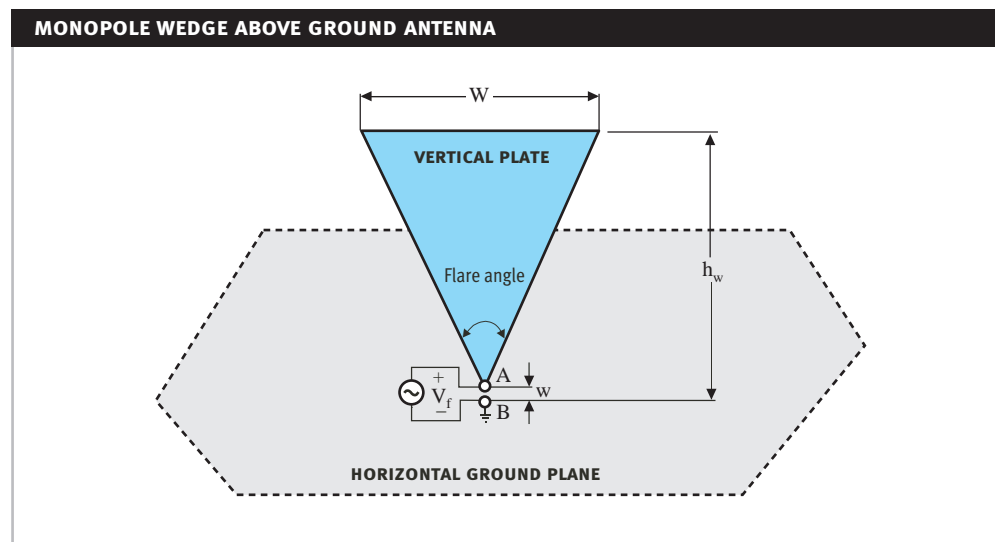


Figure 1b: The practical construction of the monopole wedge above ground antenna tuned and matched to a 50Ω input impedance using a tapped inductor.

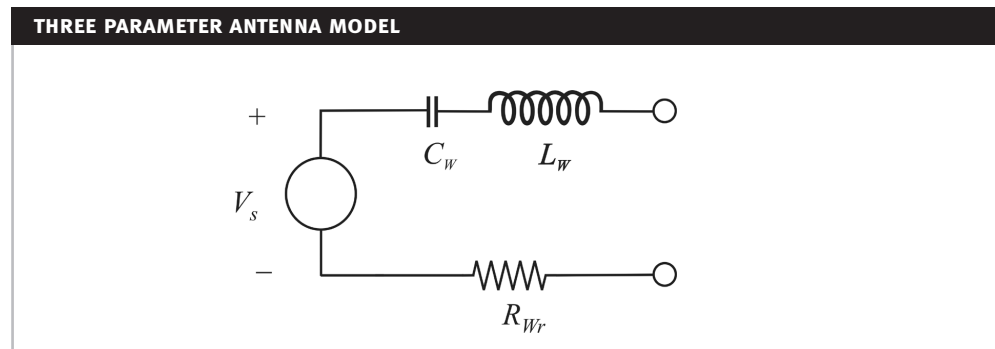


The model parameters for C_W and L_W can be conveniently obtained from the reactance $X(\omega)$ plot of the monopole wedge above ground antenna. From the circuit model of Figure 2 the reactance is given by

$$jX_W = \frac{1}{j\omega C_W} + j\omega L_W.$$

The two reactive parameters may be obtained by the frequency of intersection of the reactance with the horizontal axis, and the slope of the reactance curve at that point. Brown and Woodward's experimental results for the radiation resistance of monopole wedge above ground antennas have also been used to produce a value for the radiation resistance R_r , identified in Figure 2. Both of these calculations have been performed for different antenna heights and flare angles.

Figure 2: A three parameter equivalent circuit model for a monopole wedge above ground antenna.



The model parameters obtained will vary for different flare angles of the wedge. However, within the range of validity of the equivalent circuit, which depends upon the dimensions of the structure in relation to a wavelength, the radiation resistance, the capacitance and the inductance can be expected to scale up with increasing height for a specific flare angle. The following Table 1 provides generic expressions for the evaluation of the radiation resistance, the capacitance and the inductance values for a monopole wedge of ninety degree flare angle.

Figure 3: Reactance values obtained for a monopole wedge above ground antenna with a flare angle of 90 degrees and height h_w as indicated in Figure 1.

— Model Parameter Estimate
 — Experimental Results

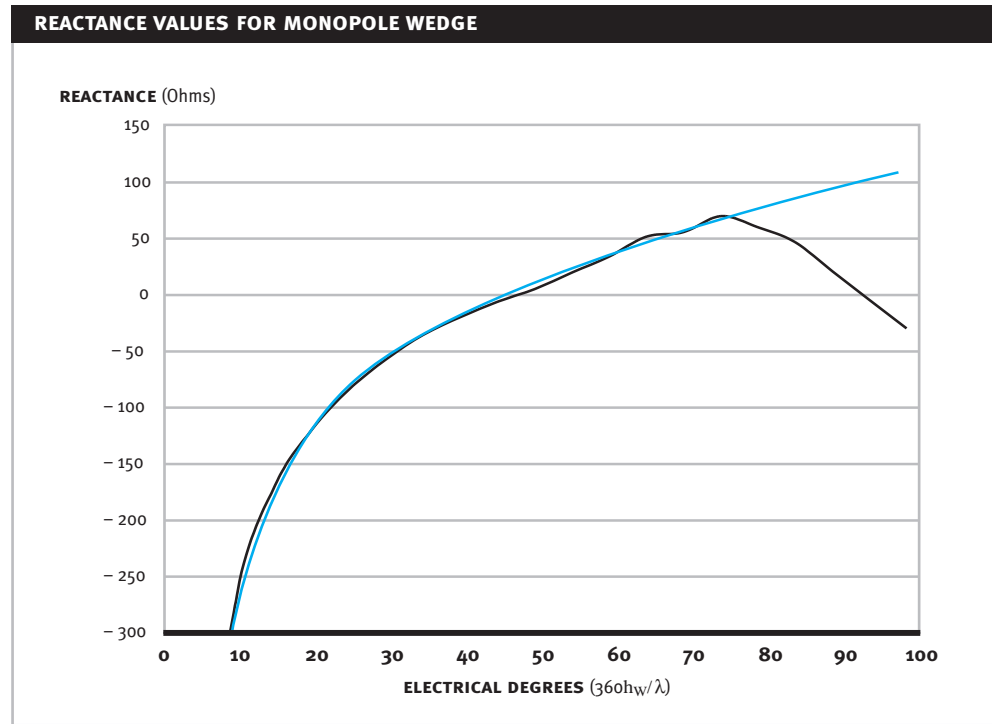


Table 1: Expressions for evaluating monopole wedge above ground antenna parameters.

EXPRESSIONS	
Capacitance (C_w) in Farads	$K_{WC} \epsilon_0 h_w$
Inductance (L_w) in Henry	$K_{WL} \mu_0 h_w$
Radiation Resistance (R_{WR}) in Ohms	$K_{WR} (\beta h_w)^2$

In Table 1 the constants K_{WC} and K_{WL} are dimensionless quantities while K_{WR} is measured in Ω . The specific values of the constants K_{WC} , K_{WL} , and K_{WR} depend on the flare angle of monopole wedge above ground. The values $K_{WC} = 7.60$ and $K_{WL} = 0.2135$ were obtained for flare angles of 90° .

The graph in Figure 3 shows a comparison between the measured reactance values for a 90° flare angle monopole wedge above ground and the reactance determined using the expressions indicated in Table 1 along with the previously mentioned values for K_{WC} and K_{WL} , while, a set of values for K_{WR} derived from Brown and Woodward’s results is provided in Table 2.

Table 2: Table of flare angles and radiation resistance constants for a monopole wedge above ground antenna of height h_w .

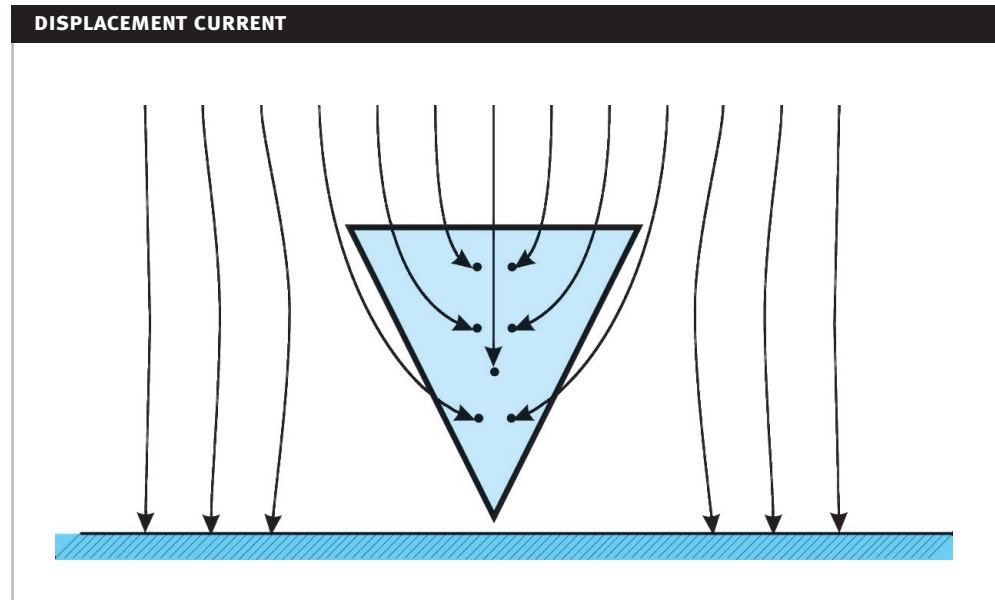
FLARE ANGLE	K_{WR} IN Ω
5	15
10	18
30	23
40	25
50	27
90	30

All of these results agree with the results of our own direct measurements of wedge reactance and radiation resistance.

Measured self capacitance values of monopole wedge above ground antennas, confirmed by our own numerical analysis performed using the method of moments has lead to a significant finding. In accord with expectations, it has been observed that the low frequency impedance of a monopole wedge above ground antennas is mainly capacitive and thus the value of the capacitance C_W in the model provided in Figure 2 can be obtained by calculating the self-capacitance of the monopole wedge above ground.

The radiation resistance obtained has significance in two ways. It allows the amount of radiated power to be calculated for a transmitting antenna, and also provides for a label antenna a means of calculating, using the Lorenz reciprocity theorem, the effective electric displacement current collecting area, as depicted in Figure 4, of the antenna. It should also be noted that in light of the reciprocity theorem, the radiation resistance is a direct indication of the capacity of the wedge to collect displacement current from a uniform applied vertical electric flux density.

Figure 4: Illustration of the electric displacement current collecting area of a monopole wedge above ground antenna.



However the application of the model in Figure 2 and the derived expressions are only suitable for electrically small antennas obeying the strict limit of

$$h_w \ll \frac{\lambda}{6}$$

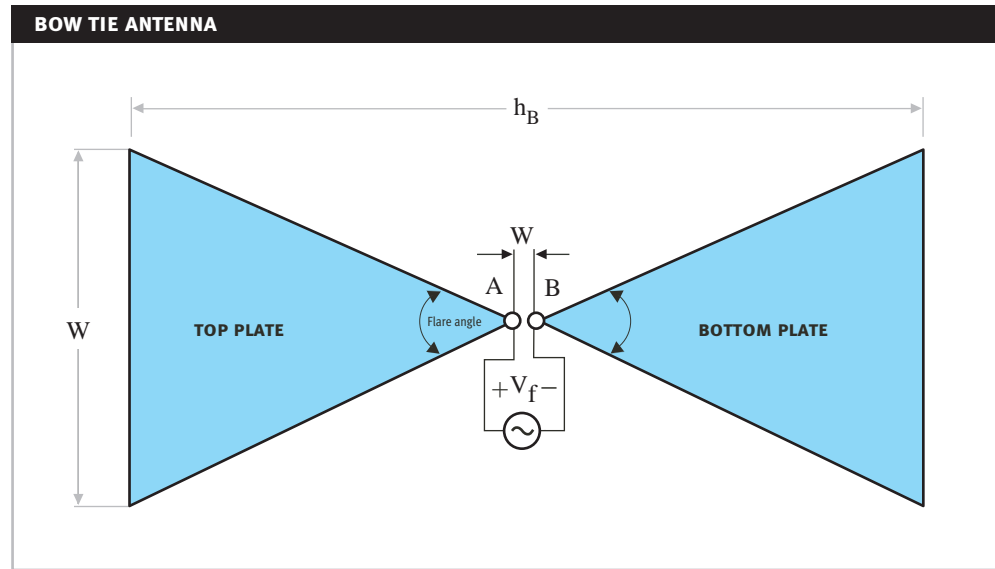
where h_w is the height of the antenna as indicated in Figure 1 and λ is the wavelength, measured in meters.

It is important to note that these results can be directly extended to analyse bow tie antennas using the method of images.

3.2. Bow Tie Antennas

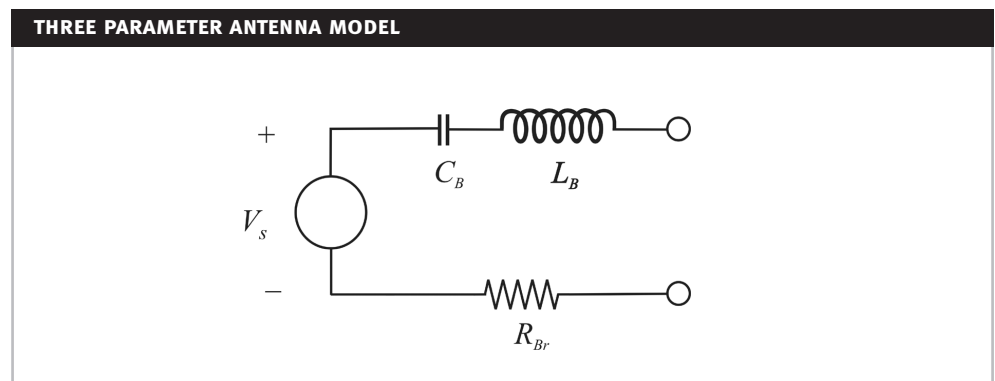
A bow tie antenna may be thought of as a construction of a monopole wedge above ground where the perfect ground plane is removed and the image under the ground plane is replaced by a physical structure as illustrated in Figure 5.

Figure 5: Bow tie antenna with the height h_B measured from the top of the top fan to the bottom of the bottom fan.



Hence, similarly to the analysis in Section 3.1 a three parameter model for the bow tie can also be represented by the model provided in Figure 6 with a radiation resistance R_{Br} , a capacitor C_B , whose value is that of the self-capacitance of the bow tie, and an inductor L_B placed in series.

Figure 6: A three parameter equivalent circuit model for a bow tie antenna.



The radiation resistance, the capacitance and the inductance variation for a bow tie antenna can also be summarised by the general expressions provided in Table 3 where the height h_B refers to the height of the bow tie antennas as depicted in Figure 5.

The expressions for the bow tie antenna circuit model parameters are explicitly stated in Table 3. In Table 3 the constants K_{BC} and K_{BL} are dimensionless quantities while K_{BR} is measured in Ω . The specific values of these constant depend on the flare angle of the bow tie and they can be derived

from the analysis of a monopole wedge above ground antenna with the same flare angle. The relationship between these values for the bow tie and wedge antennas are summarized in Table 4.

Table 3: Expressions for evaluating bow tie antenna circuit model parameters.

EXPRESSIONS	
Capacitance (C_B) in Farads	$K_{BC} \epsilon_0 h_B$
Inductance (L_B) in Henry	$K_{BL} \mu_0 h_B$
Radiation Resistance (R_{Wr}) in Ohms	$K_{BR} (\beta h_B)^2$

Table 4: Relationship between the bow tie antenna constants and the monopole wedge above ground antenna constants described in Section 3.1

RELATIONSHIP BETWEEN BOW TIE ANTENNA CONSTANTS AND THE MONOPOLE WEDGE	
Bow tie antenna constants	Numerical value of the bow tie antenna constants in terms of the related monopole wedge above ground plane antenna constants
K_{BC}	$K_{WC}/4$
K_{BL}	K_{WL}
K_{BR}	$K_{WR}/2$

However as a consequence of deriving the bow tie antenna constants from the analysis of a monopole wedge above ground antennas, the application of the model in Figure 5 and the derived expressions are only suitable for electrically small antennas obeying the strict limit of

$$h_B \ll \frac{\lambda}{3}$$

where h_B is the height of the antenna as indicated in Figure 5 and λ is the wavelength.

3.3. Loop Antennas

3.3.1. Overcoming Problems of Small Loop Antennas

Loop antennas are of significant importance at HF frequencies (13.56 MHz). The primary purpose is to create strong near fields without excessive far field radiation. The analysis of small circular loop antennas, where the term small implies that the dimensions are such that the perimeter of the loop are much smaller than the wavelength λ , can be found in [5], [6] and [7] where it is shown that the radiation resistance of a small loop antenna is given by

$$R_r = 20\beta^4 A^2$$

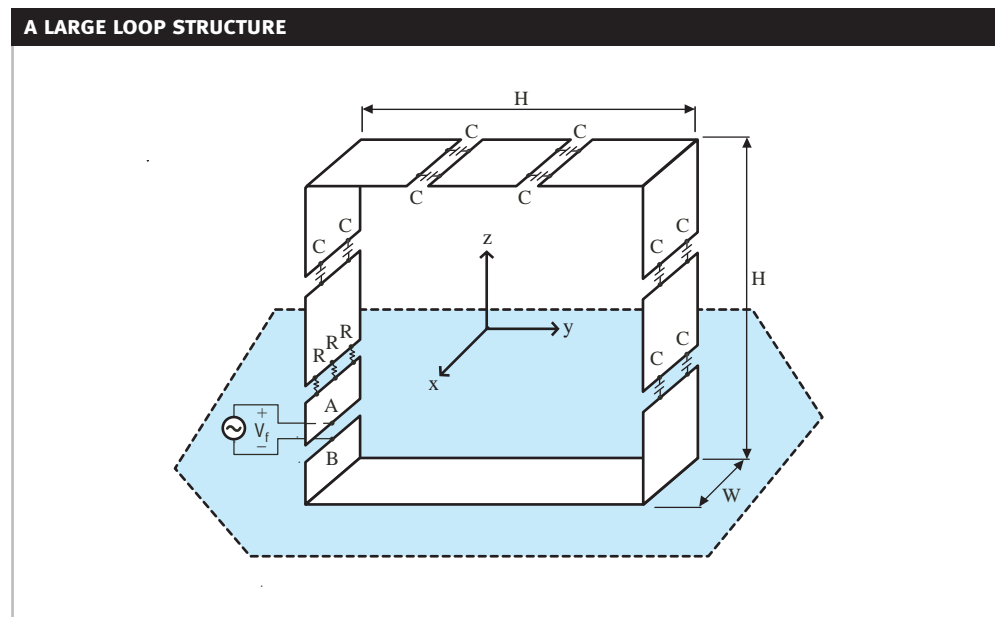
where β is the propagation constant and A is the area of the loop. It should be noted here that the radiation fields and the radiation resistance of small loops are independent of the shape of the loop and depend only on the area of the loop [9] hence the above formula can be applied to a loop of any shape as long as its area is known, and its perimeter is only a small fraction of a wave length. Also the radiation from a small loop is a maximum in the plane of the loop and is zero along its axis. The maximum radiated far-field electric field from a magnetic loop in the direction containing the plane of the loop is, in Vm^{-1}

$$E = \frac{120\pi^2 I_0 A}{r\lambda^2}$$

where I_0 is the peak current of sinusoidal excitation, r is the distance from the loop, and A is the area of the loop.

Derivation of the above result assumes a uniform current distribution over the perimeter of the loop antenna. This assumption is justified if the loop is electrically small, so that the current distribution, which must vary sinusoidally as a function of position around the loop, with the wavelength of that sinusoidal variation being equal to the free space wavelength for electromagnetic fields at the same frequency, is approximately uniform. If the current distribution around the loop is not uniform, the cancellation of the radiation from different current elements which occurs for certain radiation directions, such as the polar direction, does not occur, and the loop begins to radiate in that direction as a result of the current non-uniformity. There is also an increase in the radiation in other directions. The result is that the electric field expressed above becomes the limiting far-field electric field, that is, it is the minimum value of electric field that occurs as a result of the loop radiation.

Figure 7: A large loop structure designed to achieve a uniform current distribution.



The discussions in [1] introduced a large loop structure, shown in Figure 7, which can still be considered as an electrically small antenna at 13.56 MHz, because an effort was made to keep the current distribution uniform despite the loop's considerable size. The construction of large loops according to this design overcomes characteristic limitations of electrically small antennas: high radiation antenna quality factor, small bandwidth and high input impedance sensitivity to changes in frequency, and another practical consequence of small antennas: high and possibly unused energy density per unit volume created close to the loop centre, so that the real power required to drive the antenna becomes large [1].

However, the analysis of large loops requires careful consideration. The results presented above are for electrically small antennas with perimeters much less than a wavelength. However as the perimeter of a loop antenna become a sizable fraction of wavelength, it is important to consider the consequences of the results obtained by Pocklington that shows the current distribution on thin wires to be sinusoidal, to a very good approximation, with a wavelength of the sinusoidal variation being equal to the electromagnetic wavelength in free space at the operating frequency. Hence, an increase in a perimeter of a loop towards the 22m value of the wavelength at 13.56 MHz demands that the true nature of the current distribution on a loop be taken into consideration. As discussed above, a direct result of the non-uniform current distribution is an increase in the far-field radiation. With a balanced feed, the magnitude of the current follows a cosine distribution function with the maximum opposite the feed point. Figure 8 illustrates a loop with the black section representing the physical structure of the loop and the thickness of the

blue section representing the current magnitude. The magnitude of the current I along the loop will vary according to

$$I = I_0 \cos(\beta l)$$

where l is the linear position on the circumference with $l = 0$ opposite the feed point, and I_0 being the maximum value of the sinusoidal current excitation.

Figure 8: The distribution of current magnitude around a loop.

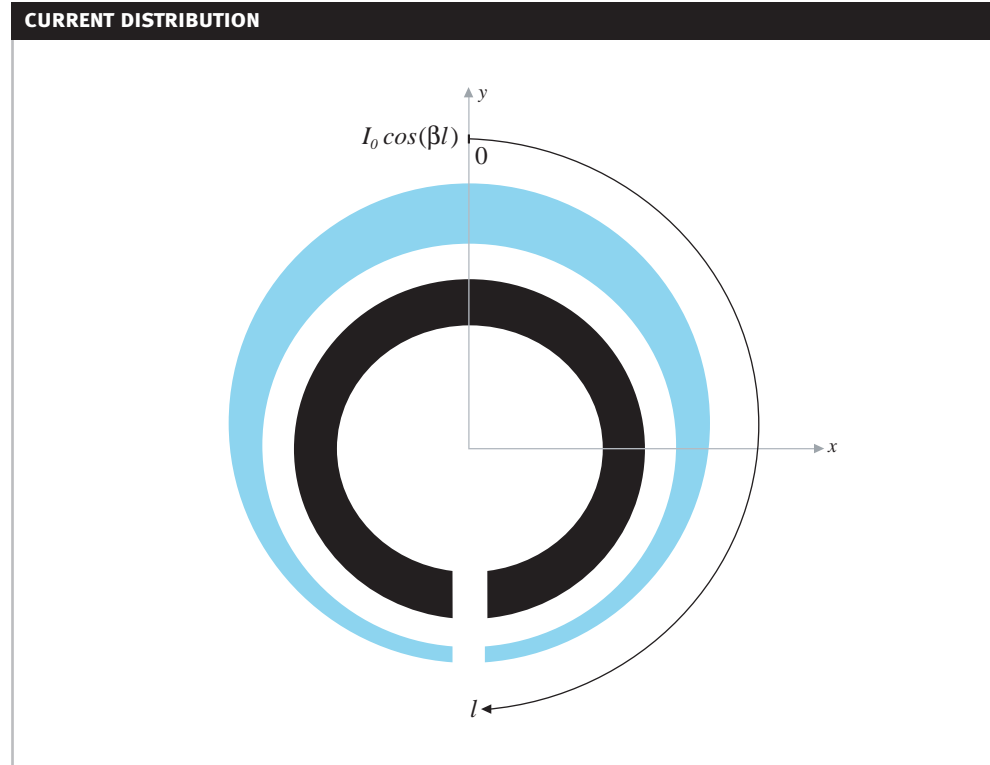


Figure 8 allows the effect of non uniform current distribution on far field radiation to be explained qualitatively. As far as radiation along the polar axis is concerned, the vertical sections of loop have approximately equal magnitude and oppositely directed currents, and continue to cancel in their effect upon radiation in the polar direction. However, the current at the feed point is substantially less than the current opposite and these currents no longer provide such cancellation, so radiation in the polar direction begins to occur.

Considering now radiation in the equatorial plane, the points to the right of the loop or the left of the loop do not produce a great contribution in the far field radiation as the current elements on the left and the right sections of the loop have the same magnitude, hence the net radiation after superposition is due to the fact the two groups of current are at different distances from the far-field point, and suffer a different phase delay in radiating thereto. However if a far-field position above the loop is considered then the current elements on the bottom of the loop pointing left are further away from the current elements on the top of the loop pointing right, but in this case the element on the bottom have a lesser magnitude than the current elements on the top, so the net radiation after superposition is due to the residual currents on the top both being closer to the far-field point and also having a larger net magnitude (the reduction from the other side of the loop is less).

Thus we see that the unbalanced currents on sections of the loop will act in a manner similar to a small electric dipole. Hence the radiation patterns in the far field will be similar to those produced by small electric dipoles and the electric and magnetic field vectors created by the unbalanced current can be evaluated using the far field solutions of an electric dipole [1], with a current element of size IL given by the unbalanced current I and the length of the section of the loop containing the unbalanced current. The strongest radiation produced will be polarized along the x axis.

It is possible to estimate the unbalanced current of two parallel sections of a square loop by considering the current distribution around the loop to be sinusoidal. Figure 9 illustrates the current distribution around a loop of perimeter $\lambda/4$. Clearly the currents on the left and the right sections of the loop are not unbalanced due to symmetry. However there is a significant variation in the net current on the top and the bottom section of the loop. The product of IL for the unbalanced current can be found by the difference between the current integral along the top and the bottom of the loop, where the sinusoidal current distribution is given by

$$I_0 = \cos(\beta l).$$

The difference in the current length product will radiate in a manner similar to having a short dipole of length $\lambda/16$ at the center of loop, aligned along the x axis. The unbalanced current IL thus calculated is

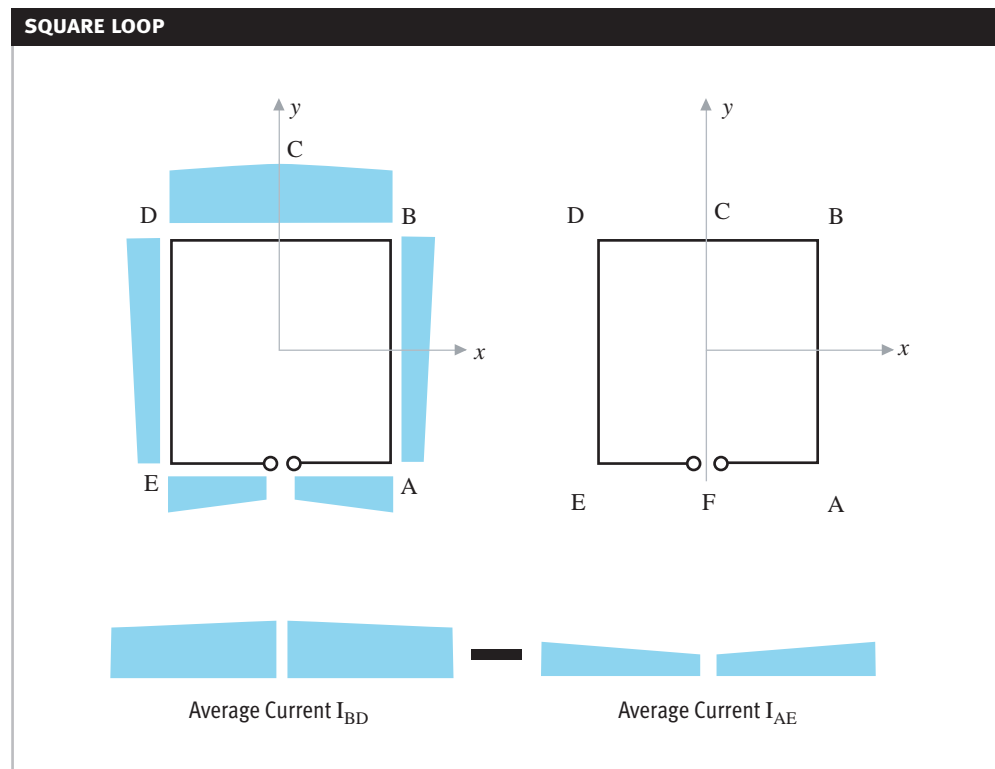
$$IL = \frac{0.1I_0}{\beta}.$$

Substitution of the current length product in to the short dipole's strongest far field electric field yields the result

$$E_x = \frac{0.1\beta I_0 \eta}{4\pi} \left(\frac{j}{\beta r} \right) e^{-j\beta r}.$$

As stated previously, the strongest radiation from the short dipole will be polarized in the x direction.

Figure 9: The current distribution around a loop of perimeter $\lambda/4$ in free space. The size of the loop considered is similar to the size of the loop discussed later in Section 3.3.2.

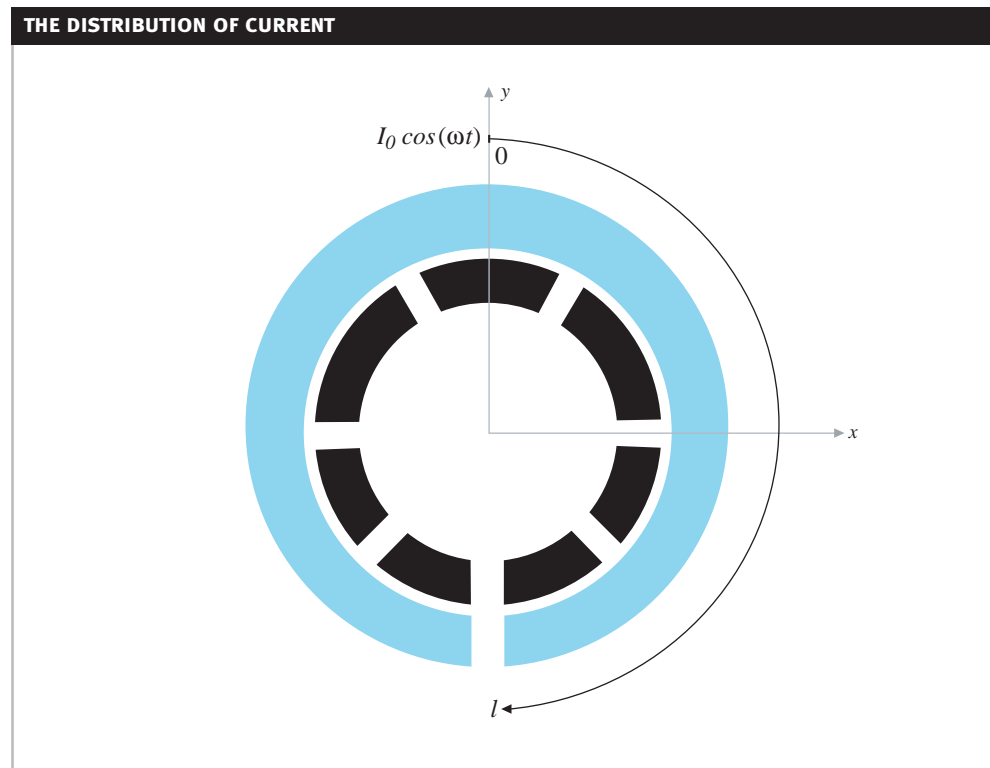


The method for reducing the far-field radiation of a practical magnetic loop thus stems from the effort to keep the instantaneous magnitude of the current distribution around the loop uniform. If a loop is segmented as shown in Figure 10, and is supplied with equal excitation at each of the gaps, the current distribution of a segment of a loop can be considered as having a maximum at the centre of the segment, taken as being the local origin $l = 0$, and an even distribution function following

$$I = I_0 \cos(\beta l)$$

as the linear dimension l is traversed. With this segmentation, the variation in current magnitude in each segment follows that of the cosine function near its maximum, i.e. the amount of change of current in each segment is small, as the segment lengths are small.

Figure 10: The current magnitude distribution around a segmented loop.



The segmentation of Figure 10 is implemented practically by physically cutting the loop into small sections with the electrical connection maintained by the insertion of a capacitor between each section. The value of each capacitance is chosen such that the combined value of all capacitances in series is that required to resonate the inductance of the uncut loop at the frequency of excitation. By way of approximation, one of the feed points is supplied with a voltage generator that has the job of supplying the voltage drop across the radiation resistance. Since this voltage drop is much less than the voltage drop across the loop inductance we have obtained a practical approximation to the symmetrically fed loop described earlier. A practical construction of such a loop and its analysis is presented in the following section.

3.3.2. Practical construction of a large loop antenna

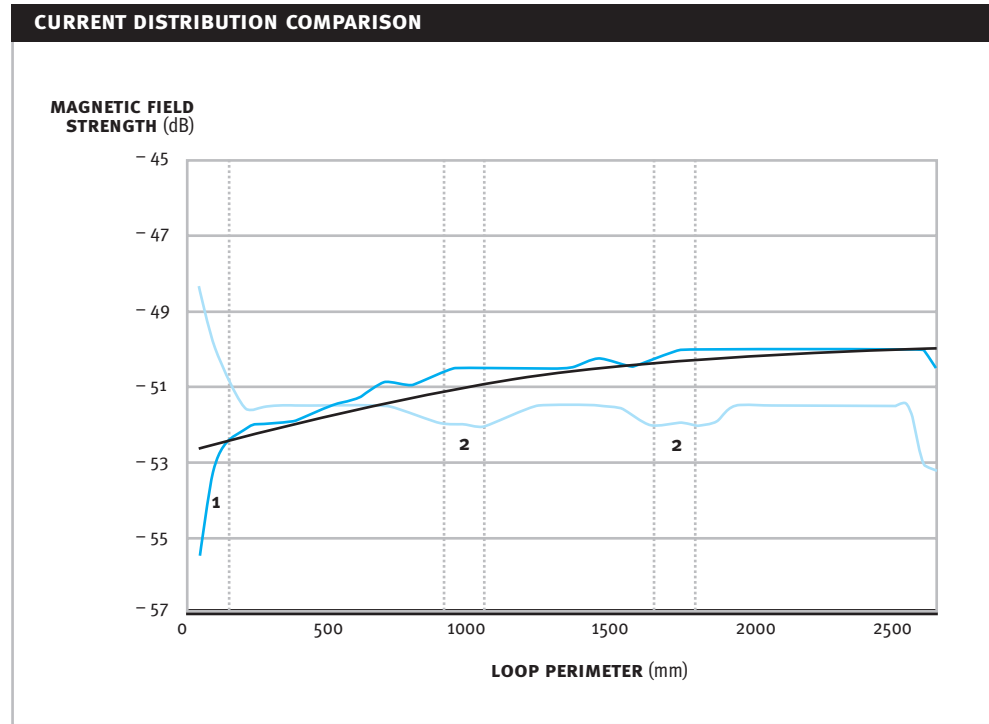
Figure 11: Large loop construction



As just described, the large magnetic loop with the distributed capacitance should allow the current to be distributed more uniformly so that the assumption of uniform current distribution made in the analysis of physically small loop antennas is still true for physically large and no longer electrically small loop antennas.

Figure 12: Comparison of the current distribution around a large loop and a slotted loop with the expected sinusoidal current distribution.

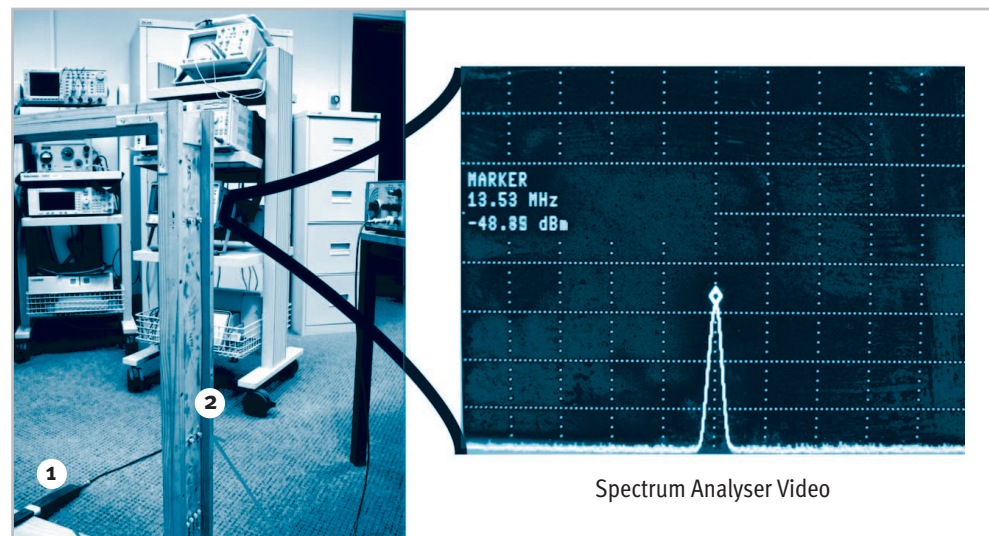
- 1 Feed Point and Corner
 - 2 Corner
- Averaged
 - Expected sinusoidal current distribution
 - Loop with slots and a network of capacitors



The relative magnetic field strength plot shown in Figure 12 was obtained by using a HP11841A close field magnetic probe connected to a spectrum analyser with a video averaging detector operating over a 10 MHz bandwidth around a centre frequency of 13.7 MHz, to record the variation of magnetic field close to the loop as the probe is moved around the perimeter of the large loop shown in Figure 11. Figure 13 shows the instrumentation set up used to obtain the above graphs. The tendency of the large loop with no capacitive slots can be clearly seen to follow the sinusoidal current distribution expected around the loop. The breaking up of the continuous loop structure into slots has achieved a remarkably uniform current distribution.

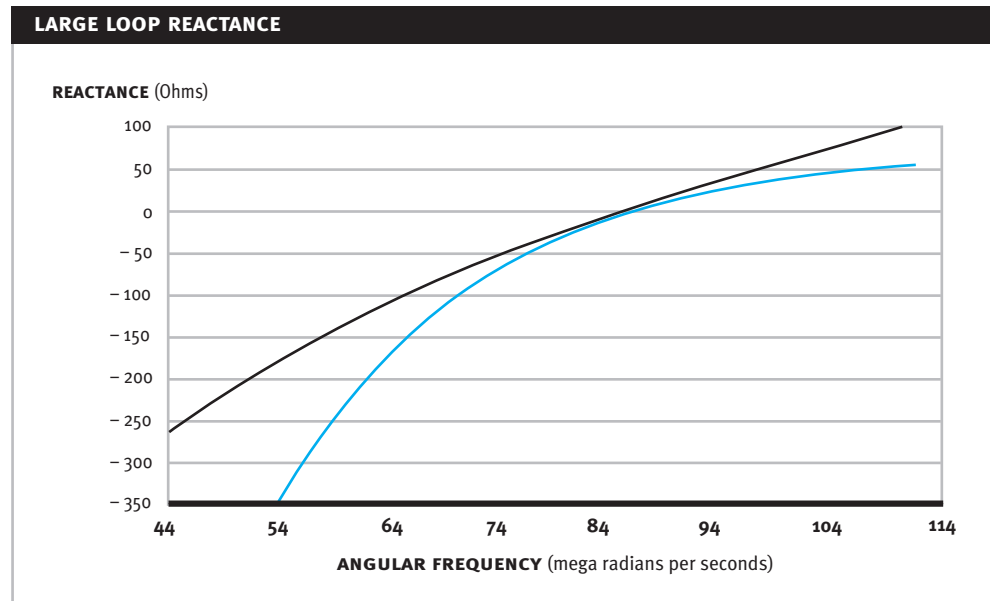
Figure 13: Instrument set up used for obtaining the magnetic field around the loop using a close field magnetic probe.

- 1 HP Magnetic Probe
- 2 Large Loop Structure



As an illustration, the modelling of the loop antenna shown in Figures 7 and 11 and the extraction of useful parameters is discussed below. The loop shown has been tuned to 13.47 MHz and matched to a 50 Ohm input impedance at resonance through the insertion of a series resistor at one gap.

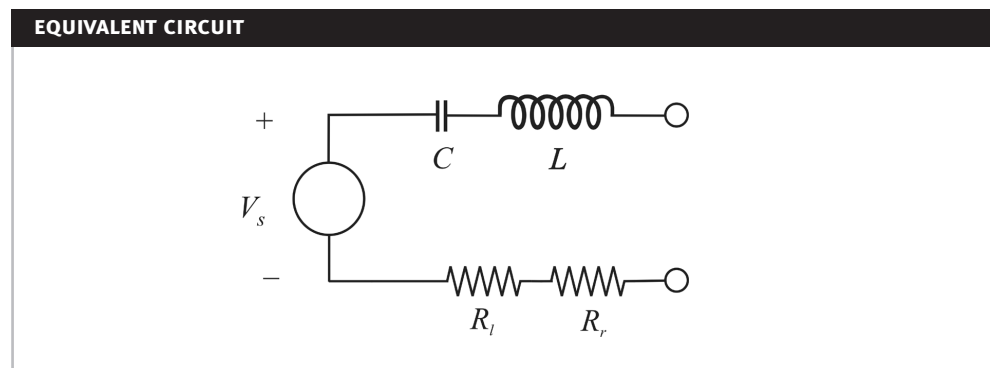
Figure 14: The graph shows the comparison between the measured reactance and the reactance estimated using the equivalent circuit modelling parameters.



An equivalent circuit for the loop antenna can be developed by using the reactance curve shown in Figure 14 to obtain the capacitance, C and the inductance, L of the equivalent circuit given in Figure 15 (detailed information on antenna equivalent circuits can be found in [1]). Figure 14 also shows the resulting reactance obtained using the model parameters C and L derived from the measured reactance. Thus the reactance of this loop can be modelled as

$$jX_L = \frac{1}{j\omega 63.1\text{pF}} + j\omega 2.21\mu\text{H}.$$

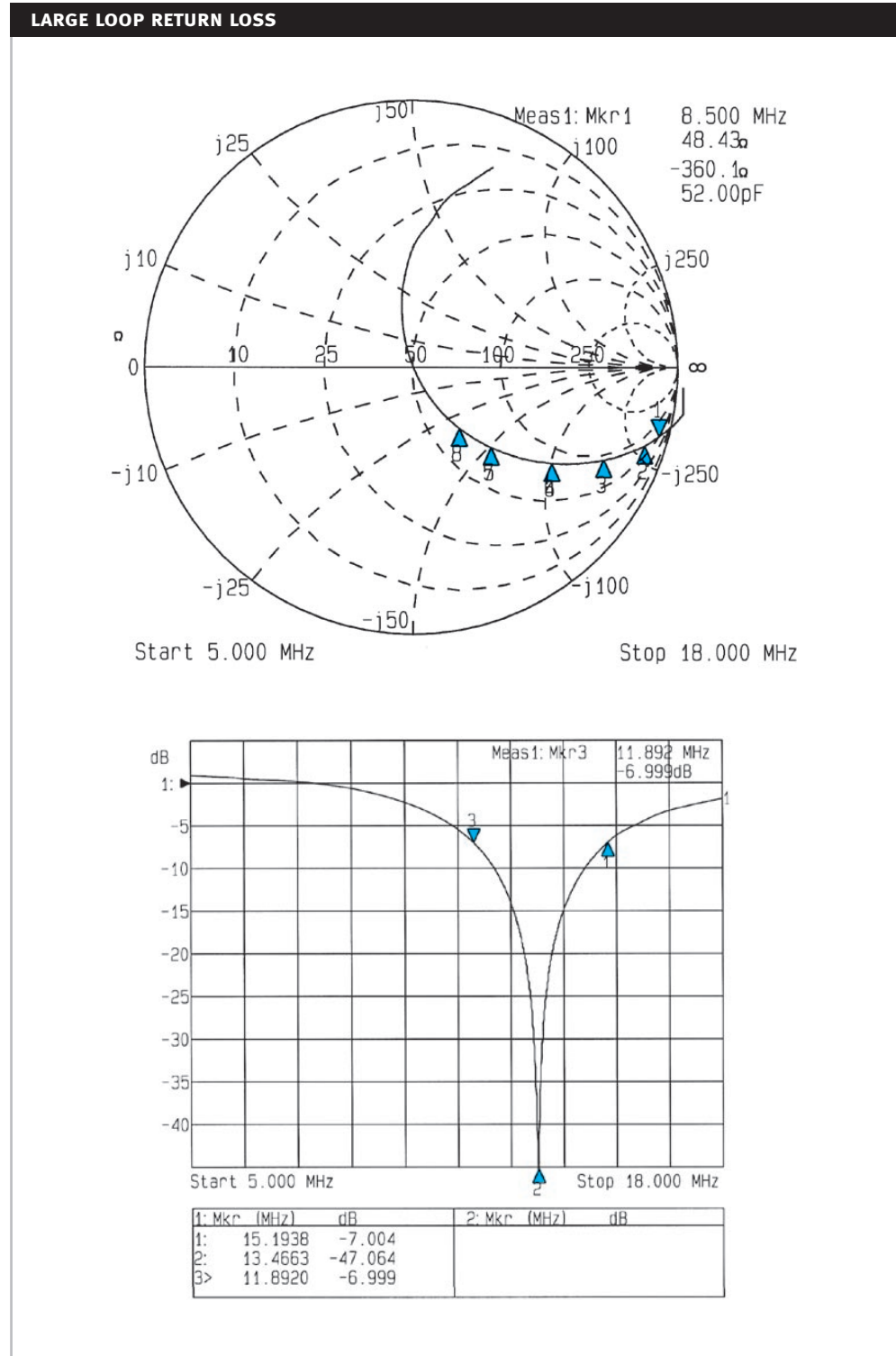
Figure 15: Equivalent circuit model for the large loop antenna.



The radiation resistance of the loop can be estimated on the uniform current assumption by using the formula for radiation resistance R_r of a small loop antenna provided in Section 3.3.1. Since the area of the loop is 0.76 m^2 the radiation resistance of the loop is approximately 0.2 Ohms. The ohmic losses

in the loop represented by R_l on the equivalent circuit are due to the added series resistance of 49.8 Ohms. As the input impedance is known, a voltage measurement at the feed point of the antenna can be used to predict the antenna current and hence on the uniform current assumption the radiated power from the antenna.

Figure 16: The Smith chart shows the variation of the impedance of the large loop antenna across a frequency range of 5 MHz to 18 MHz while the return loss curve obtained clearly indicates resonance at 13.47 MHz and provides a means to calculate the bandwidth of the antenna.



The quality factor for the antenna resonance can be obtained by using a return loss plot from a network analyser as has been shown in Figure 16. It may be shown that for deep dips at resonance, the half power points of the resonant circuit correspond to the 7dB return loss points, from which the bandwidth of the resonant circuit can be computed. Thus the quality factor Q of resonance can be obtained as

$$Q = \text{Bandwidth} / \text{Resonant Frequency}$$

provides a Q of about 4 for this loop.

We emphasise that this low quality factor has been achieved through the addition of series damping resistance, and that only a small amount of the power delivered to the loop is actually radiated. As the function of the loop is the creation of near field, this is a good thing.

4. COUPLING VOLUME THEORY

The concepts encompassed by coupling volume theory and the formulation of the coupling volumes both in electric field and the magnetic field antennas can be found in [1] and [2]. The application of the theory has special importance in the design of RFID systems. Some useful applications of the concepts are (a) to compare the performance of different forms of antenna, and (b) to illuminate the dependence of the coupling volume parameters and other operational parameters on the antenna size.

Prior to illustrating an application of the theory it is appropriate to introduce and consider another related performance parameter, namely the radiation quality factor Q_r of an antenna defined as

$$Q_r = \frac{\text{Impedence of the self-inductance (or capacitance) at resonance}}{\text{Radiation resistance of the antenna}} .$$

It has already been shown in [1] that an electrically small antenna's performance is adequately characterised by its coupling volume, which is related to the physical dimensions of the antenna. The radiation quality factor is a performance parameter that can also be related to the physical dimensions of an antenna. The radiation quality factor is important because it establishes the bandwidth over which efficient communication is possible, even in the absence of antenna losses.

An application of these concepts to well shaped planar electric and magnetic field label antennas can be illustrated by considering a single turn loop antenna structure and a bow tie antenna, each constructed from a square of size l as shown in Figure 17 and 18.

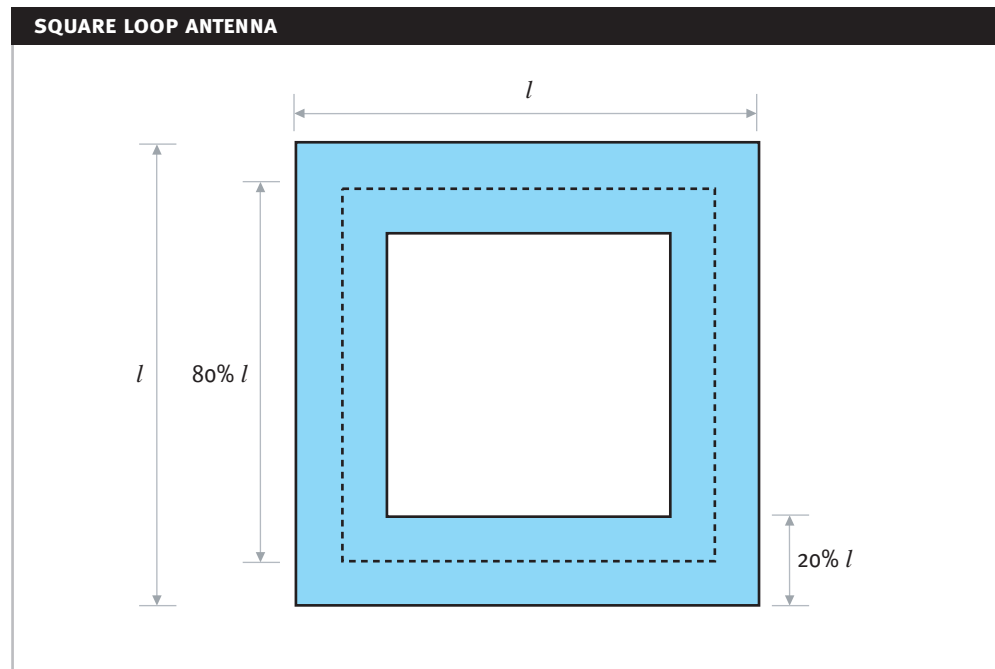
4.1. Loop Antenna Structure

The self-inductance of a small single-turn circular coil of diameter D made from wire of diameter d is, given by [7]

$$L = \frac{\mu_o D}{2} \left[\log_e \left(\frac{8D}{d} \right) - 2 \right] .$$

The construction of a square coil is depicted in Figure 17.

Figure 17: A square loop antenna created from a square of length l .



The inductance formulae above is assumed to be approximately applicable to a single turn planar square coil using a number of assumptions: the area of the equivalent circular coil of diameter D is equal to the area of the square marked through the centre of the strips forming the square coil, and the diameter d of the circular wire is half width of the strips forming the square coil.

A derivation of the radiation quality factor for the magnetic field sensitive loop antenna formed with a square of side l may be obtained using this result for the self inductance and using the radiation resistance calculated on the uniform current assumption. The result is

$$\text{Magnetic } Q_{Mr} = \frac{40}{(\beta l)^3} .$$

It has been presented in [1] that for a planar coil, which in its idealised state has no physical volume, the coupling volume is given by

$$V_c = \frac{\mu_0 A^2}{L}$$

where A is the flux-collecting area (incorporating by summation an area for each turn) of the coil, and L is the self inductance. For the loop presented in Figure 17 it can be shown after evaluation of the self inductance that that the coupling volume for the loop is

$$\text{Magnetic } V_{Mc} = \frac{1}{2} l^3 .$$

4.2. Bow Tie Antenna Structure

An analysis of bow tie antennas is given in Section 3.2 and further results can be obtained from [8]. These results can be successfully applied to calculate the radiation resistance and the coupling volume of the bow tie antenna constructed within a square of side l as depicted in Figure 18.

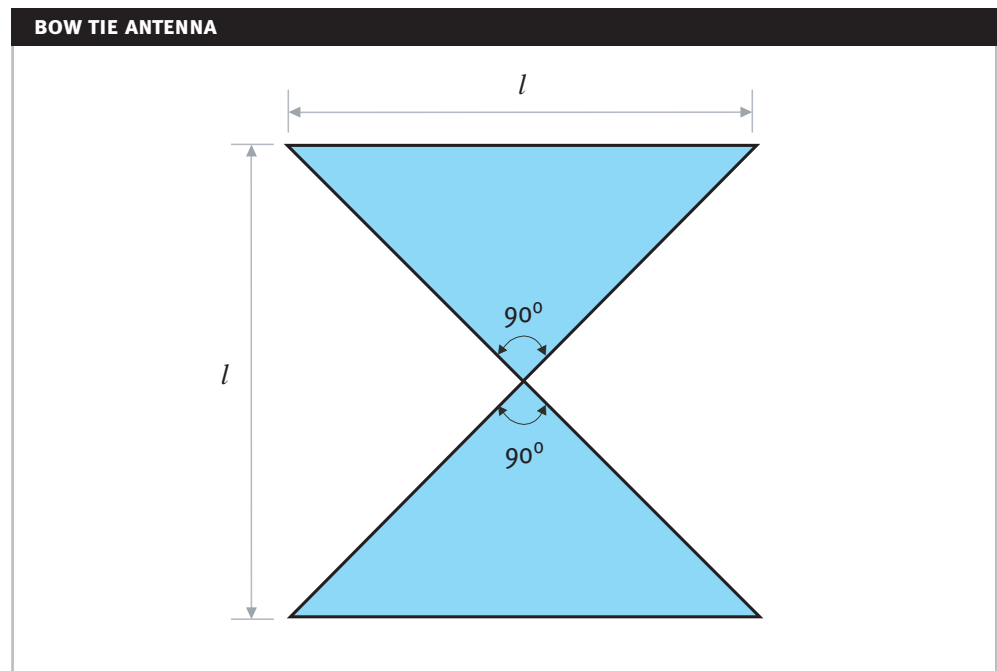
The radiation quality factor of the bow tie antenna in Figure 18 can be shown to be

$$\text{Electric } Q_{Er} = \frac{13}{(\beta l)^3}.$$

While the coupling volume of the antenna is obtained as

$$\text{Electric } V_{Ec} = \frac{2}{3} l^3.$$

Figure 18: A bow tie antenna created from a square of length l .



4.3. Antenna Comparison

For convenience we summarise the results obtained above in Table 5 below.

Table 5: Summary of coupling volume and radiation quality factor expressions.

	BOW TIE ANTENNA STRUCTURE	LOOP ANTENNA STRUCTURE
Coupling Volume	Electric $V_{Ec} = \frac{2}{3} l^3$	Magnetic $V_{Mc} = \frac{1}{2} l^3$
Radiation Quality Factor	Electric $Q_{Er} = \frac{13}{(\beta l)^3}$	Magnetic $V_{Mr} = \frac{40}{(\beta l)^3}$

The analysis that has been presented is an illustration of the application of the coupling volume theory to antenna performance measurements and to the dependence of antenna performance on physical size.

The results presented for the loop and the bow tie antenna clearly indicate that the coupling volumes and the radiation quality factor for well shaped planar electric and magnetic field labels are size dependent, but similar, and have the same order of dependence on size.

The significance of the coupling volume calculation is that it indicates how much energy can be extracted from a near or far field by an electrically small antenna. It appears that bow tie antenna has a slight superiority over loop antennas if one is not concerned at whether the energy density is created in an electric or magnetic field. The input impedance properties of RFID labels, however, suggest that loop antennas are more likely to achieve the desirable resonance than bow tie antennas unless additional tuning inductances are used.

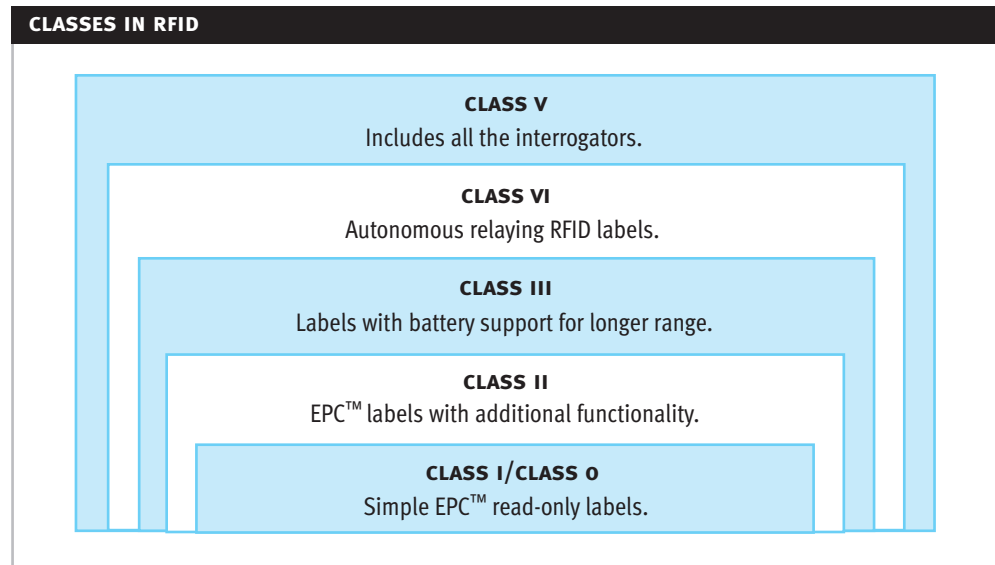
The significance of the radiation quality factor calculation is that efficient operation of grossly electrically small antennas over useful bandwidths is infeasible.

5. TURN ON CIRCUITS

The Auto-ID Centre's formulation of a label class hierarchy permits the development of labels to suit different application requirements. This is an important aspect of the development of this technology, as the environmental, functional, cost, range, security and privacy requirements will vary depending on the application employing RFID technology.

A discussion of a proposed label class hierarchy to accommodate the needs of an increasing field of RFID applications is outlined in [10] and [11]. Figure 19 outlines the proposed class hierarchy described in [10].

Figure 19: Label Class Hierarchy



The primary focus on this section of the paper is on Class III and Class IV labels that will be equipped with a power source (such as a paper battery). Class III labels are expected to be backscatter reply with the logic circuits of the labels being powered from the onboard batteries while Class IV labels are likely to be independent reply generating labels. The interrogation of Class III and IV labels will inevitably involve the development of a mechanism for turning on the labels as power conservation is an important factor that requires the labels to be turned off when not being interrogated.

A turn on circuit is a type of receiver which applies a battery power to an RFID transponder after receiving an appropriate trigger signal level. Turn on circuits will allow Class III labels to operate at greater distances than those achieved with passive labels, and also allow a well controlled trigger field to be established for active labels. The primary goal, however, is to activate the label only when required, thus conserving power and extending the life of the label battery.

5.1. Concepts

The practical options for turn-on circuits are two fold:

- rectifier circuits that can produce from an illuminating RF field a voltage of the order of 1V that can turn a CMOS transistor from fully off to fully on; or
- rectifier circuits that can produce from an illuminating RF field a voltage of the order of 10mV that can be amplified in a sub-threshold current CMOS amplifier to a level in which a transistor can be turned from fully off to fully on or can operate a sensitive comparator operating at sub-threshold current levels. Circuits of this latter type are described in [13].

For the production of a rectified output even to an open circuit load, a rectifying diode must experience across the junction capacitance a voltage of the order of or greater than the rectified output, and hence a minimum of reactive power must flow into and out of the junction capacitance. To service that reactive power, a resonant circuit must be provided and the power lost in that resonant circuit must be provided by the available source power from the antenna.

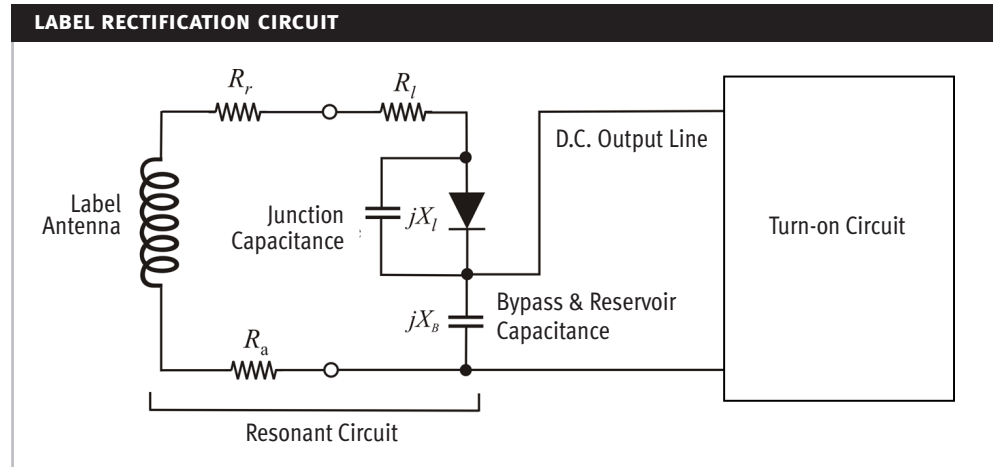
5.2. Realistic Performance Predictions

A label antenna, that in this application is preferably inductive, and the rectifying circuit that is intended to produce a rectifying voltage used for circuit turn-on, can be modelled as indicated in Figure 20. Here R_r represents the antenna radiation resistance, X_s represents the antenna reactance, X_l represents the reactance of the diode capacitance, X_B is the reactance of the reservoir capacitor that also serves as an RF bypass, R_l represents the loss in bringing reactive power into and out of the diode junction capacitance, and R_a is the ohmic loss contribution from the antenna.

The antenna ohmic losses can hopefully be ignored since the antenna construction can, in a good design, be a slot antenna containing a significant amount of copper. In addition the combination of the impedance jX_l and jX_B will be approximately equivalent to that provided by the diode junction capacitance, as the reservoir capacitor has a relatively larger capacitance of the order of 100 pF. It is assumed that no d.c. power is removed from the diode. By shaping the antenna and its connection points appropriately, an impedance match between R_r and R_l can be achieved.

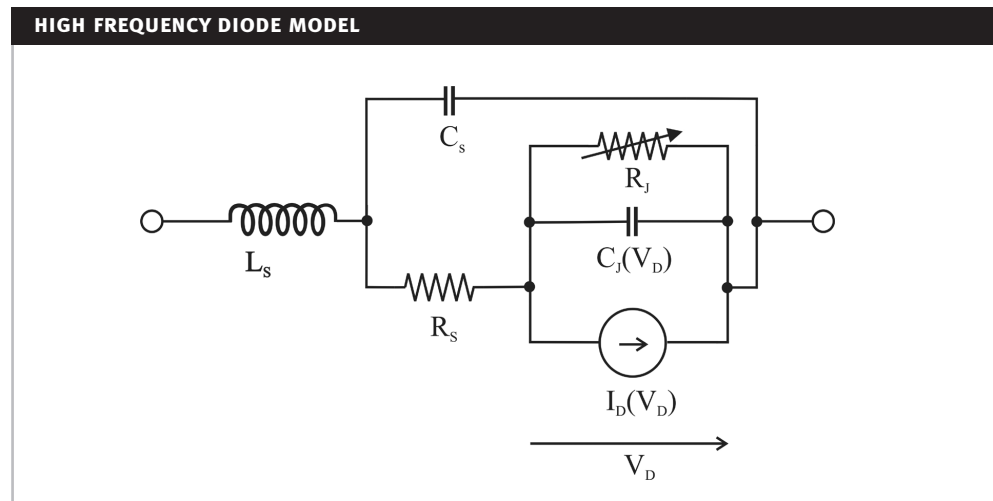
Determining the minimum power required to produce one volt across the reservoir capacitor of the label circuit requires care. The procedure involves: selecting a suitable diode; setting up an impedance matching circuit; setting up an RF rejection circuit and minimising damping caused by radiation. The following paragraphs will cover these aspects in further detail.

Figure 20



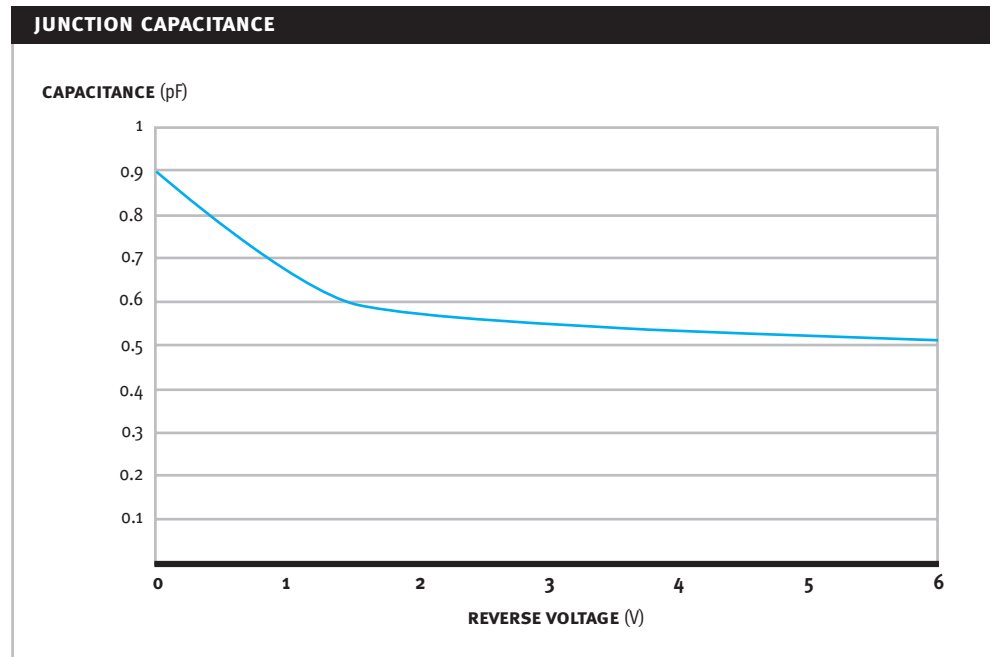
A model of a diode at high frequencies is presented in Figure 21. R_s is the parasitic series resistance of the diode, L_s is the series package inductance and C_s is the package capacitance, where the capacitance C_j which depends on the bias voltage V_D is the voltage across the junction. Current CMOS manufacturing techniques can produce small Schottky diodes with junction capacitances (diode depletion layer capacitance) ranging from 0.1 pF to 1 pF. However a Schottky junction is relatively delicate and sensitive to excessive RF power. RFID applications may work in poorly controlled environments where high power may cause the diode to burn out. Hence in an application it is important to use power limiters to protect the sensitive Schottky diode.

Figure 21



Experiments detailed in the paper utilised the Hewlett Packard 5082-2835 Schottky diodes [3] (a surface mounting version of the same diodes are available as HSMS-2820). These are a good candidates for the application due to the range of its capacitance (1pF – 0.5 pF) and low cost. Figure 22 provides a plot of the variation of the junction capacitance as a result of the reverse biasing voltage across the depletion region.

Figure 22: Variation of the diode junction capacitance as a result of the reverse voltage.



In addition, consideration must be given to practical matters regarding the construction of the circuit and the measurement of the voltage developed across the reservoir capacitor at various RF energies fed from the antenna. The circuit design must minimise damping caused by measuring instruments, connectors and radiation from physical structures such as the inductor used to represent the antenna or the leads connecting the electronic components. The issues of “hot wires”, and radiating connections and components are serious at high frequencies. Thus the construction of the experimental circuit should employ low loss and low series inductance capacitors, small coil inductors, and short connections with adequate shielding provided by a metal box as shown in Figure 23a. The shielding from the metal box serves to reflect radiated energy back into the circuit, and so reduce losses from the radiation mechanism. It also produces a small and unimportant change to the inductance and capacitance properties.

As the measurement method uses a network analyser, the RF input port of the measurement circuit requires an impedance matching network with a capacity for external adjustment. This is provided by an adjustable trimmer capacitor in series with stray inductance of the capacitor connections. Measuring the output voltage from the reservoir capacitor requires very good filtering to remove all the RF content in order to minimise radiation from the output connection before the voltage is measured across the reservoir capacitor. A schematic of the diode rectification voltage measurement circuit is provided in Figure 23b.

The impedance matching network utilised employs a capacitor in parallel with a large ($10\text{k}\Omega$) resistor (to provide a DC path across the capacitor). The impedance of the matching circuit is given in the Smith chart provided in Figure 24. The impedance appears close to the periphery of the Smith chart implying a lossless termination and from the nature of the chart it is clear that the impedance below 900MHz is capacitive while above 900MHz is inductive.

Figure 23a: Instrumental arrangement used to conduct the turn on circuit experiments. The circuit used for diode rectification studies is shielded in the metal box.

1 Test circuit shielded in a metal box

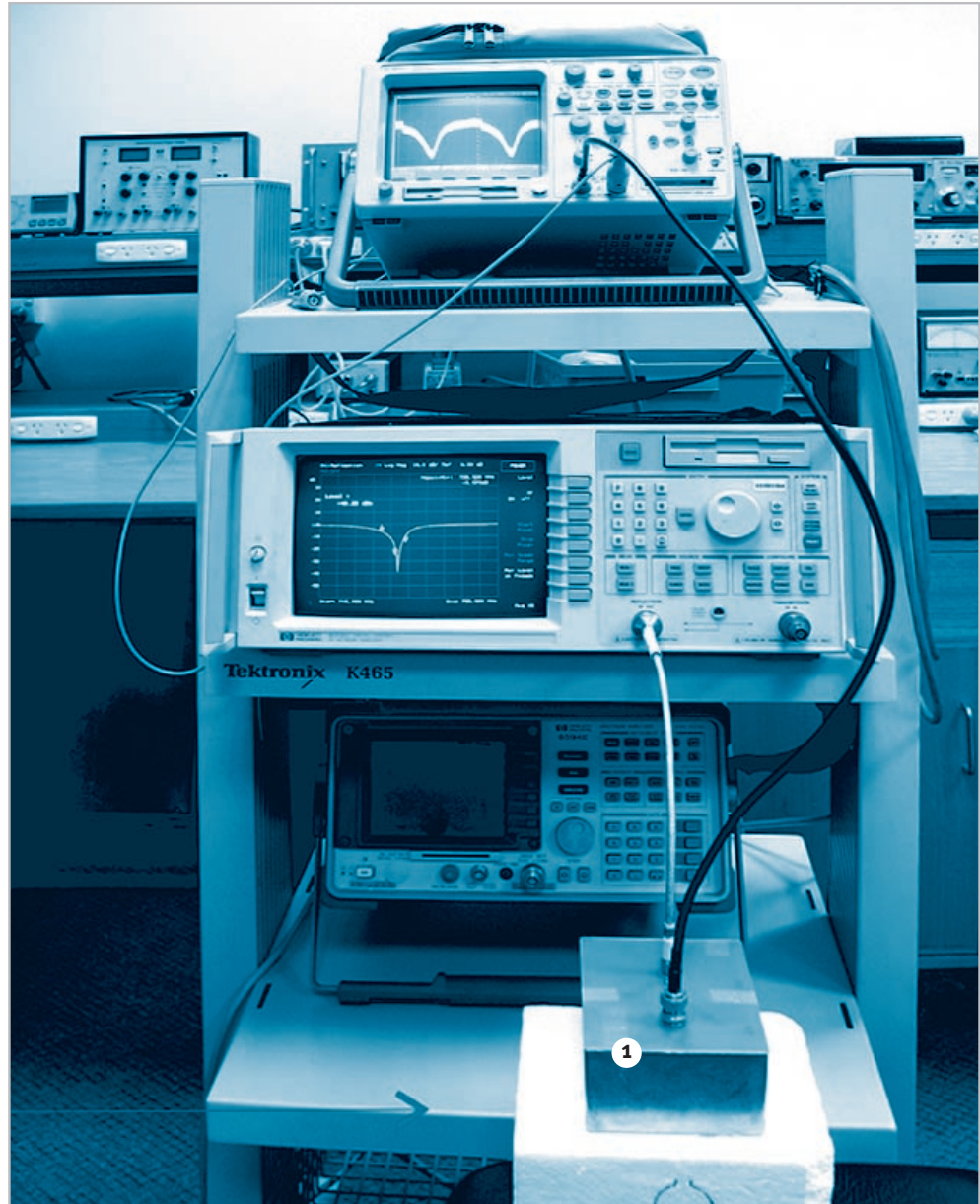


Figure 23b: The schematic of the circuit shielded in the metal box.

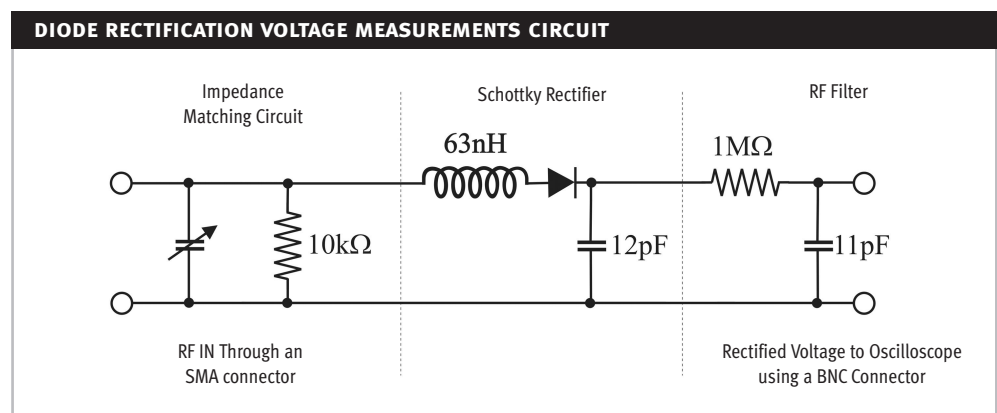
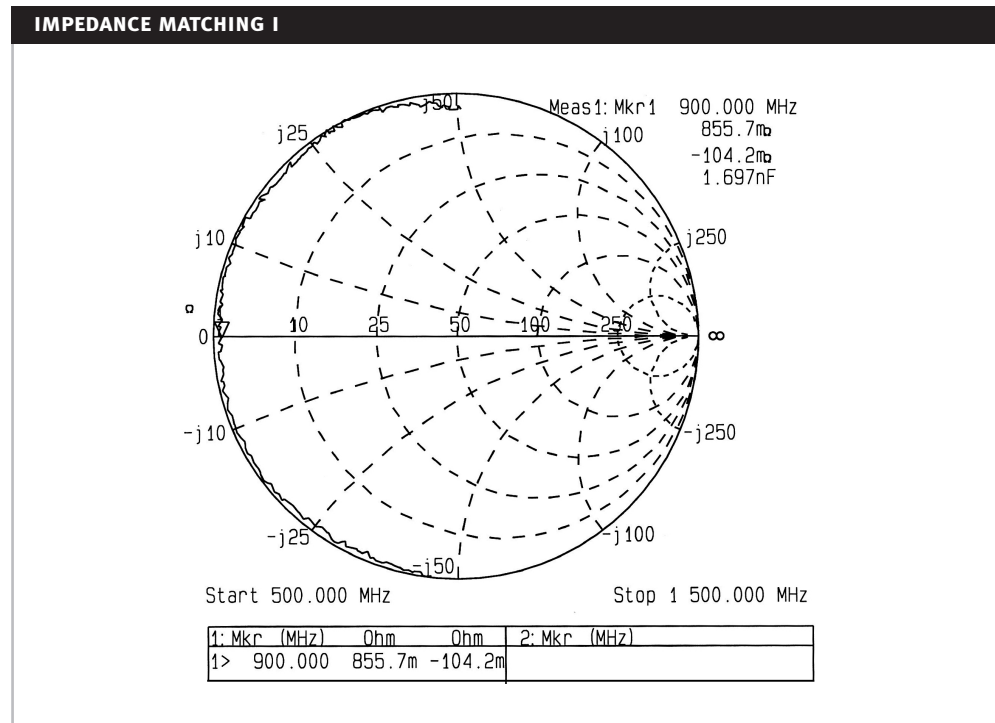
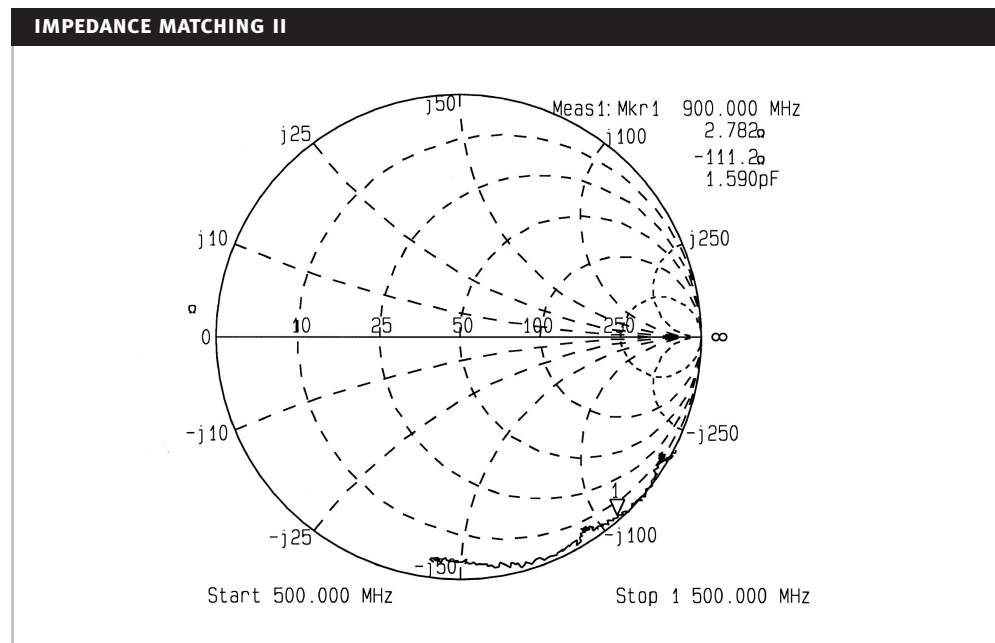


Figure 24: Smith chart of the impedance matching network showing impedance values over a bandwidth of 1000 MHz.



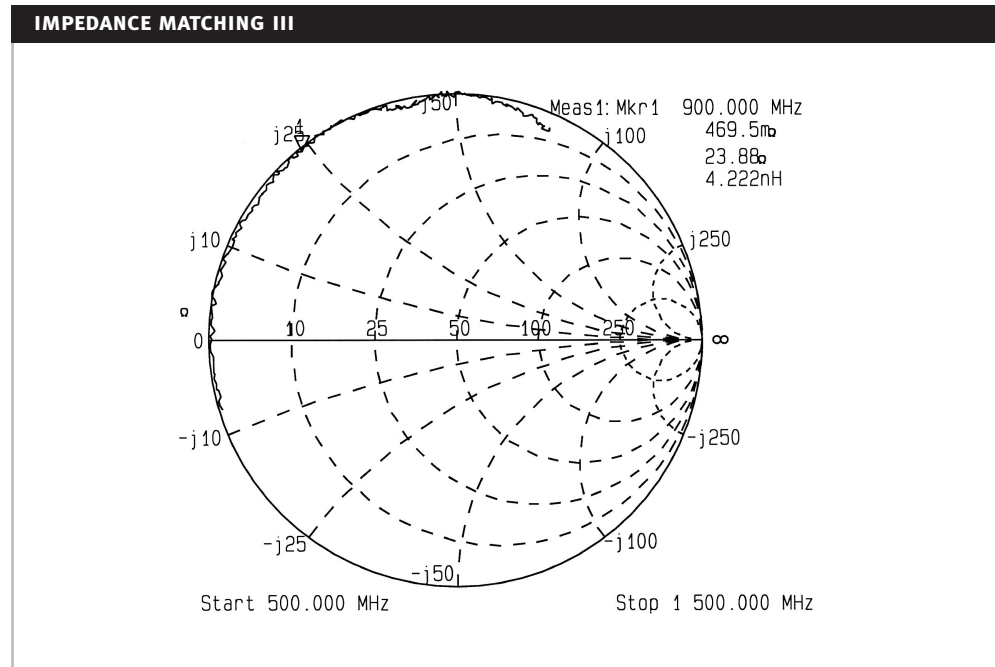
However this is not entirely true as the value of the trimmer capacitor can be adjusted to obtain a wider range of capacitive or inductive impedances as indicated in Figure 25 and Figure 26. A point of resonance for the setting that produced Figure 24 can be observed at 900MHz but at resonance the impedance of the transmission cable is mismatched to the impedance of the resonant circuit. The fact that the impedance plot is at the left edge of the Smith's chart is indicative of a detuned open circuit and hence indicates the matching network to be a series resonant circuit.

Figure 25: Smith chart of the impedance matching network showing impedance values with the trimmer capacitor set to its minimum value.



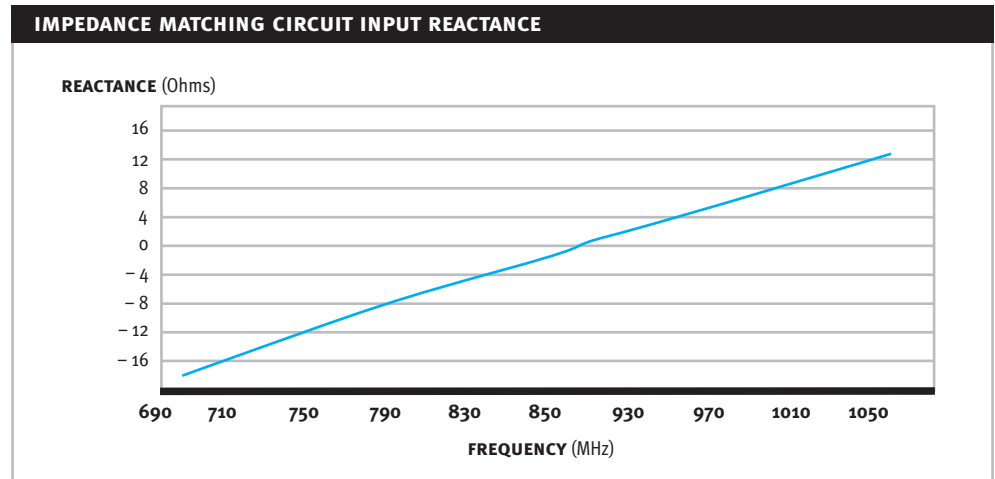
It is important to gauge the Q of this circuit as it provides an indication of the lossless nature of the impedance matching network. This is an important consideration as we require most of the RF energy to be localised in the diode resonance. Estimating the Q requires a measure of the inductance, L and capacitance, C of the series resonant circuit model. The reactance graph in Figure 27 can be used to obtain the C and L parameters of the resonant circuit. The capacitance is found to be about 5.0 pF and the inductance is found to be about 6.36 nH.

Figure 26: Smiths chart of the impedance matching network showing impedance values with the trimmer capacitor set to its maximum value



The resistance of the series resonant circuit is much less than 50 Ohms since the resulting Smith chart is at the periphery for a broad range of frequencies, this point can also be observed by examining the dynamic resistance on the Smith chart. The the quality factor of this resonance is found to be around 35, so the impedance matching network is relatively broadband in relation to the quality factors expected in the diode reaonance.

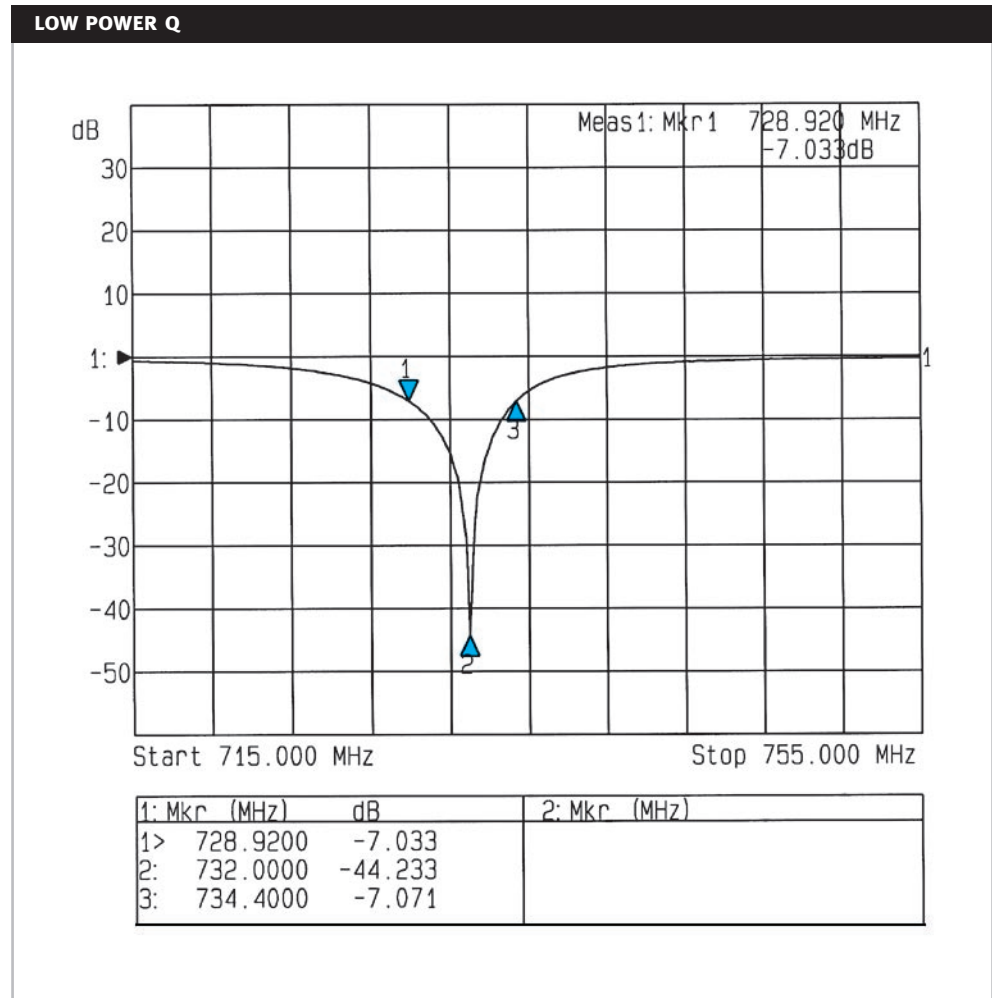
Figure 27: Reactance of the impedance matching circuit obtained using a network analyser sweeping across a frequency range of 500MHz to 1500MHz.



All of the measurements described thus far were obtained with the Schottky Rectifier and the RF Filter circuit identified in Figure 23b disconnected.

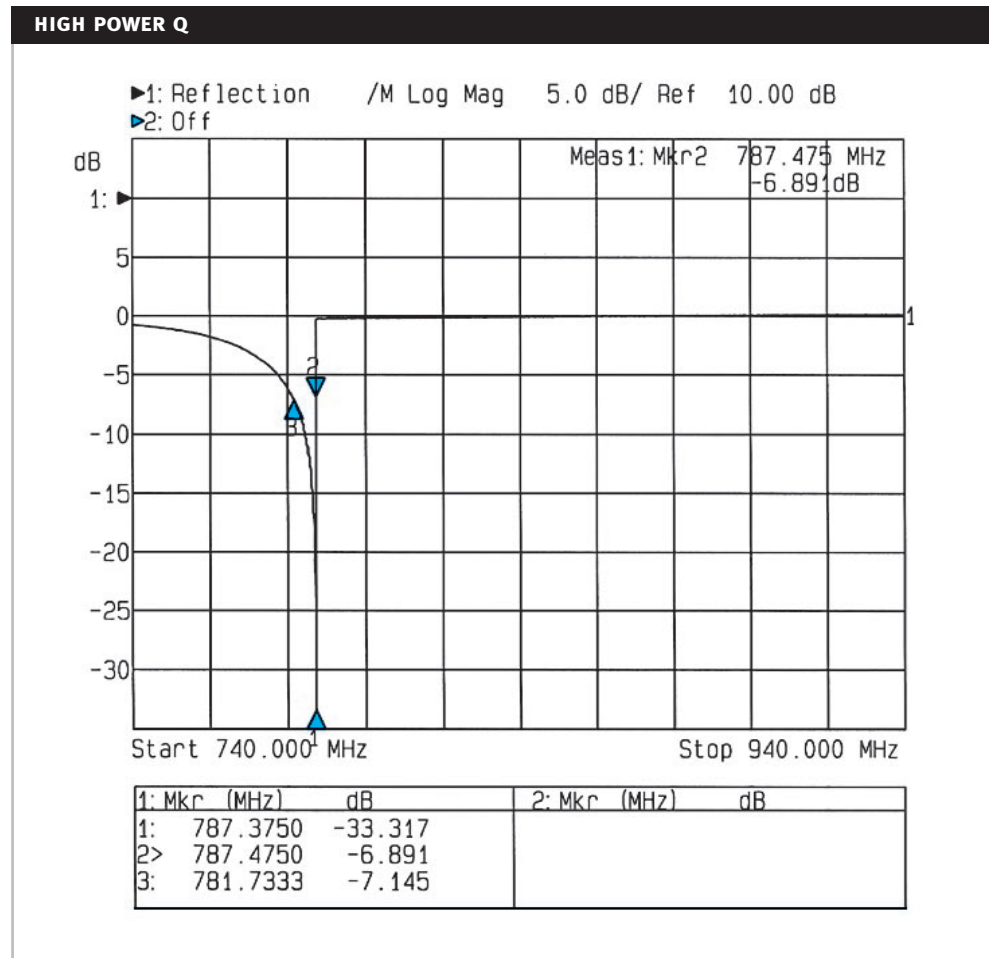
The return loss plots provided in Figure 28 with the diode connected (that is with the Schottky Rectifier and the RF Filter circuit identified in Figure 23b connected) can be utilised to obtain the low power Q of the diode resonance while the plot in Figure 29 provides a return loss curve under high power and thus can be used to obtain the high power behaviour of the diode as the source frequency is swept.

Figure 28: The return loss plot obtained with the network analyser output power level set to -35dBm indicates a low power Q of approximately 130.



The non-linearity of the circuit response at high power Shown in Figure 30 precludes a meaningful definition of high power Q.

Figure 29: The return loss plot obtained with the network analyser output power level set to -19dBm depicting the non linearity of the circuit response at high power.



5.2.1. Actual Power for Zero Power Turn on Circuit (1 V d.c. Output)

While sweeping across a large frequency range the minimum input power required to obtain a DC output of 1 volt as indicated in Figure 30 was -16.20dBm. The resulting return loss curve is presented in Figure 31 and it can be seen that over 90% of the incident power at 812MHz is feeding into the diode resonance.

Figure 30: The DC voltage obtained across the reservoir capacitor using an oscilloscope with an input impedance of 1MΩ and a capacitance of 4pF. It should be noted that the voltage observed is half the voltage across the reservoir capacitor.

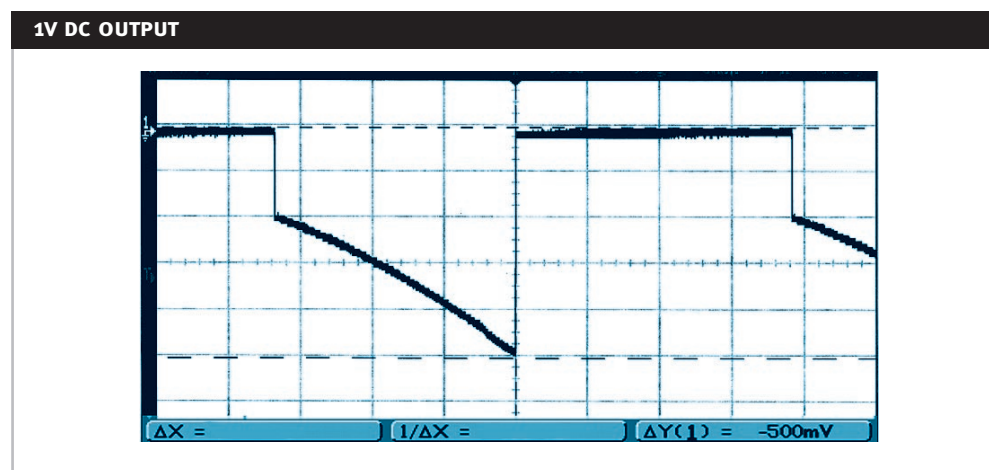
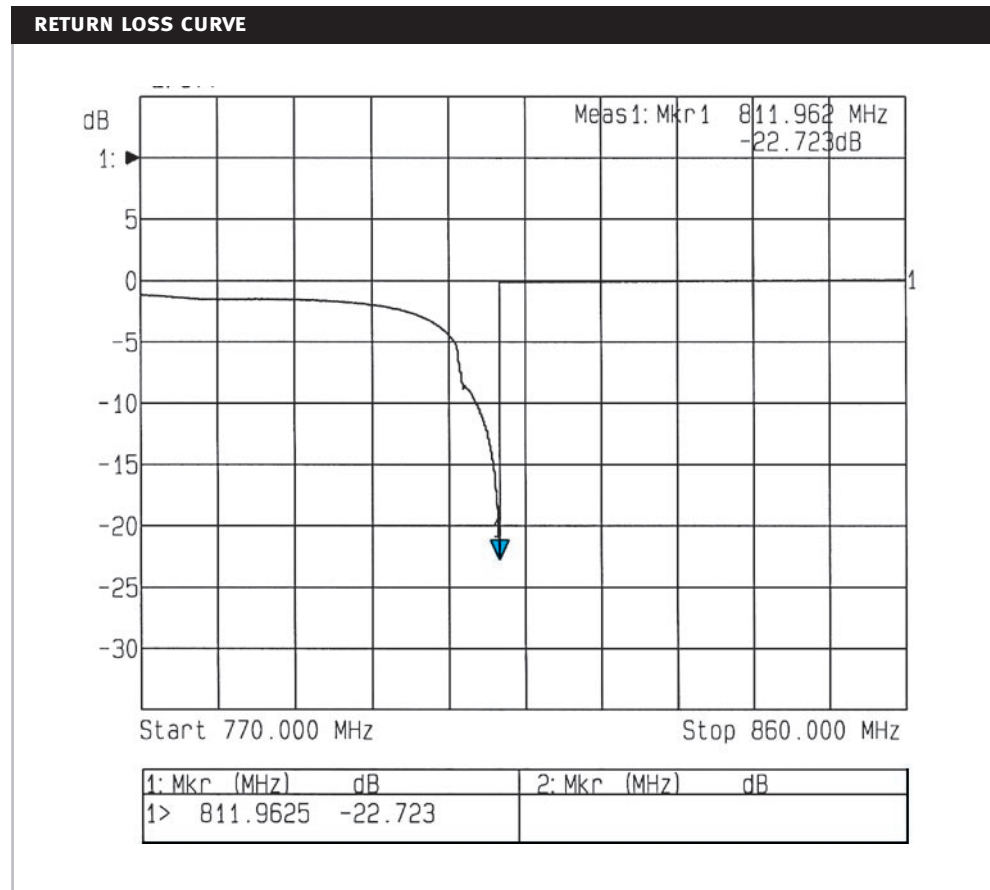


Figure 31: The return loss plot with the network analyser output RF power fixed to -16.2dBm.



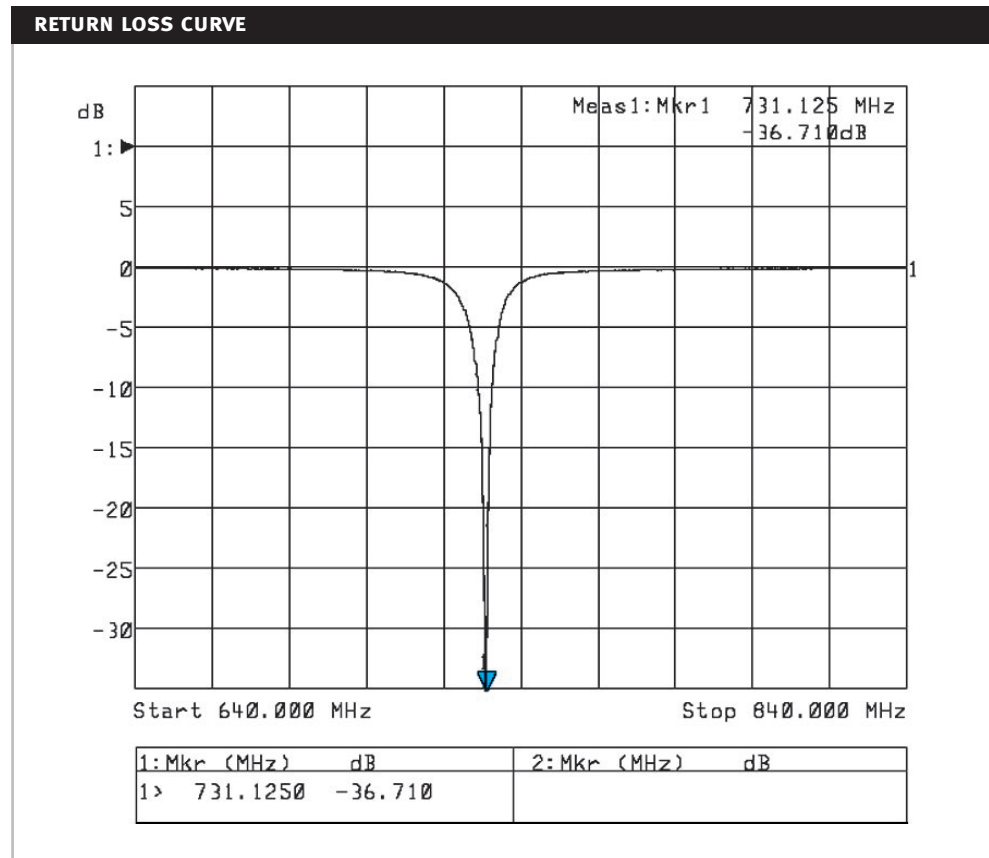
Calculation, using standard far field antenna formulae, of the range at which, for favourably oriented antennas, a reader with antenna gain of 6 dB and output power of 1W, will provide this available source power from a tag antenna of gain 1.5 gives a range of 12.6 m.

However an interesting and important phenomenon can be observed when the signal sweep bandwidth at high power is reduced. Unless the sweep begins at a frequency that is somewhere near the low power resonance frequency, and follows upward in frequency as the diode develops voltage and begins to raise its resonant frequency, the full diode output will not be obtained.

5.2.2. Actual Power for Low-power Turn on Circuit (10 mV d.c Output)

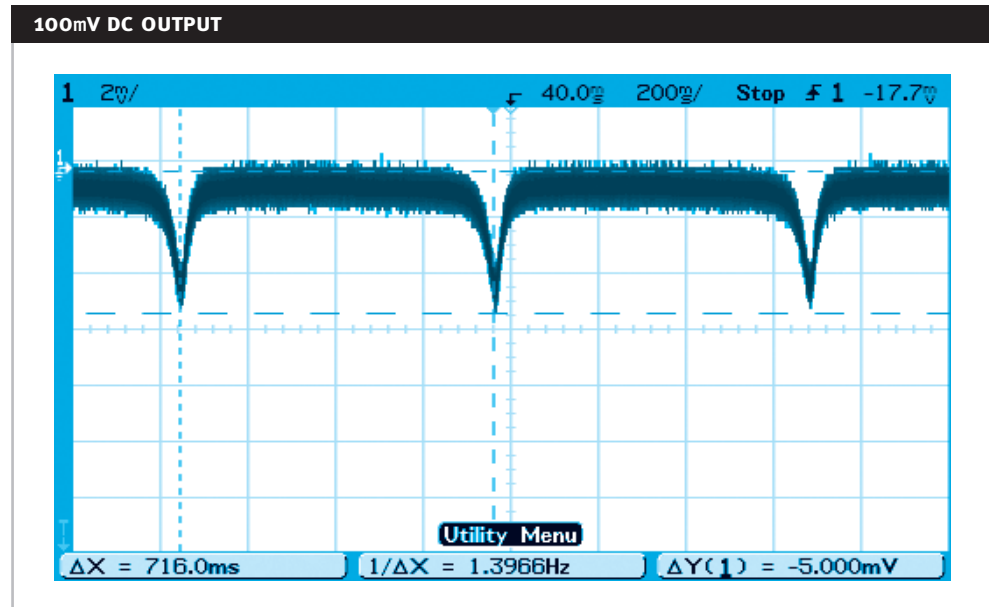
An alternative means that can still exploit the diode resonance is a turn on circuit incorporating an amplifier or a low power comparator that is permanently powered. In order for a low power turn on circuit to be useful the current drain in its “off” state must be low with respect to the self discharge current of the battery. Similar to the previous turn on circuit the present design can also be triggered by a small DC voltage, rectified and amplified by diode resonance where the minimum value will be dictated by rectified RF noise [13].

Figure 32: The return loss plot with the network analyser output RF power fixed to -43dBm with a frequency sweep of 200 MHz.



Experimental evidence has proved that a minimum RF power of -43dBm was required at resonance to obtain a 10mV DC output from the reservoir capacitor. Figure 32 shows the return loss at resonance while Figure 33 shows the voltage output from the reservoir capacitor.

Figure 33: The voltage output from the resonance circuit. It should be noted that the voltage observed is half the voltage across the reservoir capacitor.



Calculation, using standard far field antenna formulae, of the range at which, for favourably oriented antennas, a reader with antenna gain of 6 dB and output power of 1W, will provide this available source power from a tag antenna of gain 1.5 gives a range of 89 m.

6. CONCLUSIONS

Application of coupling volume theory to compare antenna performance has been illustrated using an electric field sensitive antenna and a magnetic field sensitive antenna along with the introduction of the companion concept of radiation quality factor. Thus, not only does the coupling volume theory provide insights for optimising antennas, but it can be used as a tool for comparing antenna performance. The comparison is simple, and yet powerful as it relates the many different parameters that characterise the performance of antennas to the physical dimensions of the antenna.

The development of Class III and IV labels will eventually involve the incorporation of turn-on circuits. There have been a number of novel ideas published [13, 14]; however they may not all be practicable alternatives. The concepts provided for turn on circuits in Section 6 involves the design of a turn-on circuit that functions by sweeping across a UHF bandwidth. This concept is a more practicable alternative and it is illustrated through performance measurements taken in a scenario modelling a far field, and through range predictions under favourable conditions based thereon.

7. ACKNOWLEDGEMENTS

The authors of this paper would like to thank David Hall for his insights and help in procuring instruments. Without his valuable help, completion of this paper would not have been possible.

8. REFERENCES

1. **P.H. Cole, D.C. Ranasinghe & B. Jamali, "RFID Coupling Relations".**
Auto-ID Centre White Paper, ADE-AUTOID-WH002, 2003.
2. **K. Eshraghian, P.H. Cole & A. K. Roy, "Electromagnetic Coupling in Subharmonic Transponders".**
Journal of Electrical and Electronics Engineering, Australia, 2, 28–35, March 1982.
3. **Agilent Technologies, "Schottky Barrie Diode for General Purpose Applications".**
Technical data sheet, 2003, <http://www.agilent.com>.
4. **International Organisation for Standardisation, "SI units and recommendations for the use of their multiples and of certain other units".**
International Standard ISO 1000 (1992).
5. **P. H. Cole, "Level 4 Electromagnetic Compatibility".**
Lecture notes, 2003, <http://www.eleceng.adelaide.edu.au/Personal/peter/peter/emclec.html>.
6. **O.M. Sadiku, "Elements of Electromagnetics".**
Second Edition, Saunders College Publishing, 1994.
7. **J.D. Kraus, "Electromagnetics".**
Third Edition, McGraw-Hill Series in Electrical Engineering, 1984.
8. **G.H. Brown & O.M. Woodward Jr, "Experimentally determined Radiation characteristics of Conical and Triangular Antennas".**
RCA Review, vol 13, pp 425–452, (1952).
9. **W.L. Stutzman & G.A. Thiele, "Antenna Theory and Design".**
John Wiley & Sons publishing, 1981.
10. **S. Sarma D. W. Engels, "On the Future of RFID Tags and Protocols".**
Technical Report, 2003. <http://www.autoidcenter.org/research>.
11. **P. H. Cole, "Fundamentals in Radiofrequency Identification".**
Summer Course, MIT 2003,
<http://www.eleceng.adelaide.edu.au/Personal/peter/peter/AEE/FundamentalsinRFID.pdf>
12. **Aglient Technologies, "Impedance Matching Techniques for Mixers and Detectors".**
An Application Note, 2003, <http://www.agilent.com>.
13. **D.M.Hall & P.H. Cole, "A fully integrable turn-on circuit for RFID transponders".**
Wireless and Portable Design Conference, Burlington, Massachusetts, September 1997, pp 66–71.
14. **P.H. Cole, "Coupling and Quality Factors in RFID".**
In Design, Characterisation and Packaging for MEMS and Microelectronics,
Paul D. Franzon, Editor, Proceedings of SPIE Vol. 4593, pp 1–11, (2001).

